The effect of H_2O on the vibrational populations of CO_2 in a CO_2/H_2O microwave plasma : a kinetic modelling investigation

The effect of H_2O on the vibrational populations of CO_2 in a CO_2/H_2O microwave plasma: A kinetic modelling investigation

C.Verheyen[1], T. Silva[2], V. Guerra[2] and A. Bogaerts[1]

[1]*Research Group PLASMANT, Department of Chemistry, University of Antwerp, Universiteitsplein 1, B-2610 Wilrijk-Antwerp, Belgium*
[2]*Instituto de Plasmas e Fusão Nuclear, Instituto Superior Tecnico, Universidade de Lisboa, Portugal*

Plasma has been studied for several years to convert CO_2 into value-added products. If CO_2 could be converted in the presence of H_2O as cheap H-source for making syngas and oxygenates, it would mimic natural photosynthesis. However, CO_2/H_2O plasmas have not yet been extensively studied, not by experiments, and certainly not computationally. Therefore, we present here a kinetic modelling study to obtain a greater understanding of the vibrational kinetics of a CO_2/H_2O microwave plasma. For this purpose, we first created an electron impact cross section set for H_2O, using a swarm-derived method. We added the new cross section set and CO_2/H_2O-related chemistry to a pure CO_2 model. While it was expected that H_2O addition mainly causes quenching of the CO_2 asymmetric mode vibrational levels due to the additional CO_2/H_2O vibrational-translational (VT) relaxation, our model shows that the modifications in the vibrational kinetics are mainly induced by the strong electron dissociative attachment to H_2O molecules, causing a reduction in electron density, and the corresponding changes in the input of energy into the CO_2 vibrational levels by electron impact processes.

1. INTRODUCTION

Significant efforts need to be taken to keep the warming of the earth under 1.5°C, as stated by the Paris Agreement. To reach this goal, we need to cut our carbon emissions and even try to lower the existing high levels of CO_2. Thus, the best way to battle climate change is a combined approach of reduction of the CO_2 levels and reducing the emissions.

Many approaches already exist to combat climate change, e.g., using renewable energies, carbon capture and storage (CCS), and carbon capture and utilisation (CCU), as for example, CO_2 conversion.[1] The latter has the advantage that it not only prevents CO_2 from entering the atmosphere, but it is also used as a source for value-added chemical compounds, like methanol and syngas, in line with the cradle-to-cradle principle. Moreover, since CCU can create fuels, this leads to the prevention of the extra burning of fossil fuels and of the excess CO_2 that would enter the atmosphere.

A promising method for CO_2 conversion is plasma technology.[1] It allows CO_2 conversion at mild reaction conditions (ambient pressure and temperature) because the gas is activated by electrons, which are heated by the applied electric power. Furthermore, because plasma is created by electrical power, and it is easily switched on/off, it is very promising to be used with renewable electricity, for peak shaving and grid stabilisation, to make solar fuels. Additionally, it does not require the use of scarce materials and is scalable to the size of the energy market.

Plasma-assisted CO_2 conversion has been studied already extensively.[1] The first research dated back to the late 1970s and led to a greater understanding of how to enhance the CO_2 decomposition and the effect of different plasma operating conditions.[2] It was found that vibrational excitation can be the most effective channel for CO_2 dissociation in plasma. Electrons at a temperature of T_e = 1-2 eV are very efficient in transferring energy to mostly the asymmetric stretch mode of CO_2. More than 95% of the energy can be transferred.[3,4] Microwave (MW) plasmas at reduced pressure emerged as the most energy efficient of all plasma types, with energy efficiencies of 80-90% at specific conditions.[2] The high energy efficiencies for CO_2 conversion are attributed to the relatively high electron density and low reduced electric field (E/N, where E is the electric field, and N is the gas number density), which causes the right electron temperature (1-2 eV) for selective excitation of the asymmetric vibrational mode of CO_2.[5]

Kozák and Bogaerts[6] developed a 0D chemical kinetics model for pure CO_2 conversion in MW plasmas, in which the importance of the vibrational dissociation pathway was demonstrated, and which can be used to optimise the conversion and energy efficiency.[6,7] In practice, however, CO_2 streams will rarely be in pure form. CO_2 can be captured

from fumes and exhausts or can be captured from the atmosphere, but in either way, it will be not pure, so it will need to be separated, which is an additional cost. Therefore, converting mixtures in the plasma might reduce the cost and is a more realistic representation of the actual fumes. Another advantage might be that the added gas introduces benefits for conversion and efficiency and even creates new products. Therefore, different gas mixtures have already been studied. In CO_2/N_2 mixtures,[8–11] N_2 shows beneficial effects due to the small energy difference between the first vibrational levels of N_2 and CO_2, making a fast resonance transfer of vibrational energy possible.[8,9] If we want to explore the possibilities to create hydrocarbons, such as methanol, formaldehyde and formic acid, the addition of a hydrogen source would be necessary. Therefore, dry reforming of CH_4, as well as CO_2 hydrogenation (i.e., gas mixtures of CO_2/CH_4 and CO_2/H_2) have been studied as well.[1,12,13]

A common (hydrogen-containing) gas mixture in practice is CO_2/H_2O. H_2O can be used as a cheaper and more sustainable hydrogen source than H_2. There is, however, a limited number of studies on the combined CO_2/H_2O conversion in plasmas.[14–18] Additionally, the literature data do not show consistent results. Some papers demonstrated that even small amounts of H_2O addition (1 – 2 %) yield a significantly lower CO_2 conversion, and thus a higher energy cost, compared to pure CO_2 splitting.[14–16] H_2O might quench the vibrational levels of CO_2, thus reducing the most energy-efficient conversion process. This was confirmed by studies performed in a gliding arc.[15,16] However, Chen et al.[17] reported higher efficiencies upon H_2O addition in MW plasmas, yielding a conversion up to almost 30 %, at an energy cost around 2.32 eV/molec. This MW set-up was operating at low pressures (30–60 Torr) and might, therefore, be less prone to quenching of the CO_2 vibrational levels than atmospheric pressure plasmas. In addition, H_2O might have a cooling effect, possibly increasing the thermal non-equilibrium and thus the energy efficiency. Another experimental study in MW plasma performed by Ihara et al. showed the possibility of methanol formation.[18]

The available studies[17,18] on CO_2/H_2O in a MW discharge are, however, only experimental, and there is an apparent lack of modelling studies, needed to gain a better understanding of the results. To close this gap, we extended the CO_2 model of Berthelot and Bogaerts,[19] developed for a MW plasma, with H_2O addition. For this purpose, we created a new reaction set, describing the reactions between H_2O and CO_2 and their possible products, as well as a new electron impact cross section set for H_2O. The main focus of this paper is on the influence of H_2O on the CO_2 vibrational kinetics, as this knowledge is crucial for energy-efficient CO_2 conversion in a CO_2/H_2O (MW) plasma.

2. METHODOLOGY

2.1. CREATION OF THE H_2O CROSS SECTION SET

(a) Approach

Electrons can be considered the primary agents in plasma. They are accelerated by the applied electric field and give rise to a chemically-rich environment due to collisions with heavy particles, yielding excitation of internal degrees of freedom, dissociation, and ionisation. Therefore, accurate knowledge of electron impact cross sections is of particular importance in gas discharge modelling. Cross sections are crucial for the calculation of (among others) the electron energy distribution function (EEDF), which plays an essential role in gas discharges, as it describes the probability density for an electron to have a certain energy.

In order to propose the cross sections for electron collisions with H_2O, to be used for the modelling of CO_2/H_2O plasmas, it is vital to introduce the concepts of consistent and complete sets. A set is considered complete when it can describe the main electronic processes responsible for momentum and energy losses, including those yielding changes in the number of electrons, such as ionisation. On the other hand, a set is consistent when it can reproduce measured values of swarm parameters when used as input data to evaluate the EEDF from a Boltzmann solver.[20] We use here Bolsig+[21] as the Boltzmann solver, due to its incorporation in the ZDPlasKin[22] software used in this work. Therefore, the cross section set created here was made to suit this solver.

A complete and consistent set of cross sections is often obtained adopting a swarm-based procedure.[20] A swarm of charged particles is an ensemble (collection) of particles moving through the background gas under the influence of an external electric field.[23] Therefore, swarm parameters are parameters related to the transport of electrons measured under an applied electric field. The parameters are obtained from the LXCat database[24] and Hasegawa et al.[25] Swarm parameters can be used to derive the cross sections, as well as to control the validity of the created set. The latter

procedure starts with the collection of a set of cross sections from the literature, whose magnitudes are adjusted to improve the agreement between calculated and measured swarm data. Here it is essential to mention that such a procedure does not validate the cross section of each individual process, nor it ensures the uniqueness of the whole cross section set. As a consequence, multiple sets of cross sections can provide the correct transport data. There are some ways to correct this, like obtaining more information about the relative magnitudes of the processes or putting several processes into one cross section.[26] The swarm parameters calculated in this work are the (i) electron reduced mobility and (ii) reduced effective ionization Townsend coefficient, represented by μN and αN - η/N, respectively.

(b) Creation of the cross section set

Five H_2O cross sections sets are available at the LXCat database: Triniti,[27] Itikawa,[28] Hayashi,[29] Morgan[30] and Phelps.[31] Note that another set of Quantemol was also available but included only one reaction, so it was not used in this study. Among these sets, only two – Triniti and Itikawa – were initially used. The other three lacked important rotational reactions and could, therefore, not provide good results when used in Bolsig+. Note that Bolsig+ does not allow to add populations of rotational levels in a simple way. However, the rotational levels of H_2O lie close to one another and higher levels will, therefore, be already populated at 300 K. Neither Itikawa nor Triniti sets were acceptable when compared to the experimental swarm data from Hasegawa et al.,[25] as can be seen in figure 1. From these first results (calculated at 300 K), we can conclude, from both reduced mobility and Townsend coefficient, that the Triniti set provides better results. Consequently, the Triniti set was chosen as a base set to be optimised. The Itikawa set, however, contains some interesting reactions and cross sections and was used to complete the Triniti set.

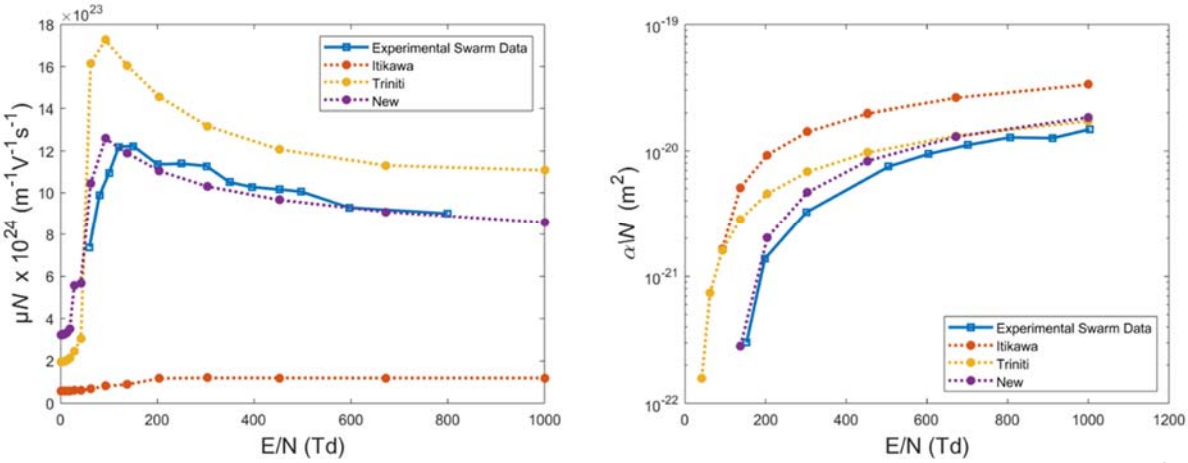

Figure 1: Reduced mobility (left) and reduced effective ionisation Townsend coefficient (right), obtained from experiments[25], and calculated with the original Triniti[27] and Itikawa[28] cross section sets, and the new set developed in this work.

To further optimise the cross section set of Triniti, a literature study was performed to find additional information about which cross sections are the most important to include and to obtain an overview about the important data sets available. In the beginning, two main review articles were consulted: Itikawa et al.[28] (as mentioned above) and Ness et al.[32] Both provide a dataset created either from reviewed or calculated cross sections. From here, some articles involving datasets,[33–35] while others related to specific processes, namely momentum transfer,[36] rotations[28,37–42] and vibrational excitation[43,44] were analysed.

The main idea is that over a range of reduced electric fields from 0 Td to 1000 Td, different cross sections have different effects. At low fields (< 35 Td) the rotational cross sections have the most significant contribution, for intermediate ranges (35 – 90 Td) vibrational cross sections are more important, and in the higher fields range (> 90 Td), ionisation and dissociative attachment are essential.[45] For polar molecules, rotational excitation is the dominant process in low energy collisions. Moreover, at energies below the vibrational threshold, the only inelastic process is rotational excitation. Thus the rotational transitions play a significant role in slowing down electrons in a molecular gas at lower reduced electric fields.[28] The rotational process with $\Delta J = 1$ is the most efficient.[38] H_2O, in general, will exhibit large rotational total cross sections, since it is a polar molecule and will, therefore, interact strongly with low

energy electrons. However, obtaining rotational cross sections experimentally can be troublesome. This happens because the rotational levels of H_2O lie very close together, and electron beam experiments do not have enough resolution to resolve each rotational state.[28] Besides, swarm experiments can give very accurate cross sections for the sum of all overlapping reactions, but only estimates of partial cross sections can be obtained.[39] If partial cross sections come into play, the use of computational methods will be a big help. Itikawa et al. used the Born approximation to derive a formula to calculate the rotational cross sections[42] that is quite in use by many authors, like Ness et al.,[32] who included around 100 calculated cross sections in their set.[32] However, more often only the cross sections up to J = 3 are included.[35,40] Sometimes, the rotational cross sections are incorporated into the elastic cross sections, creating, therefore "quasi-elastic" cross sections.[32] This delivers results that do not match with the experimental data. It is thus essential to have separate rotational and elastic cross sections.[32] Here, a combination of Itikawa's rotational cross sections was made to create one single rotational cross section.

The Triniti excitation cross sections that showed a small number of data points were replaced with cross sections that show a broader range of availability, and the number of reactions was extended (see next section). In addition, the effective cross section was replaced by an elastic cross section, that was adjusted (within the error bars) to give swarm parameters close to the experimental ones.

(c) The final cross section set

The new cross section set obtained by the above-described procedure is mostly based on the cross sections found in the LXCat database[24] and the vibrational cross sections of Seng and Lindler [46]. It consists of 13 processes that are the most important for our 0D model: (i) one elastic [29], (ii) three attachment [27,28], (iii) five ionization [28], and (iv) four excitation (including vibrational and rotational) cross sections [27,46]. These cross sections are plotted as a function of electron energy in figure 2. The swarm parameters calculated with this new set are in sufficient agreement with the measured data, for the purpose of this work (see figure 1).

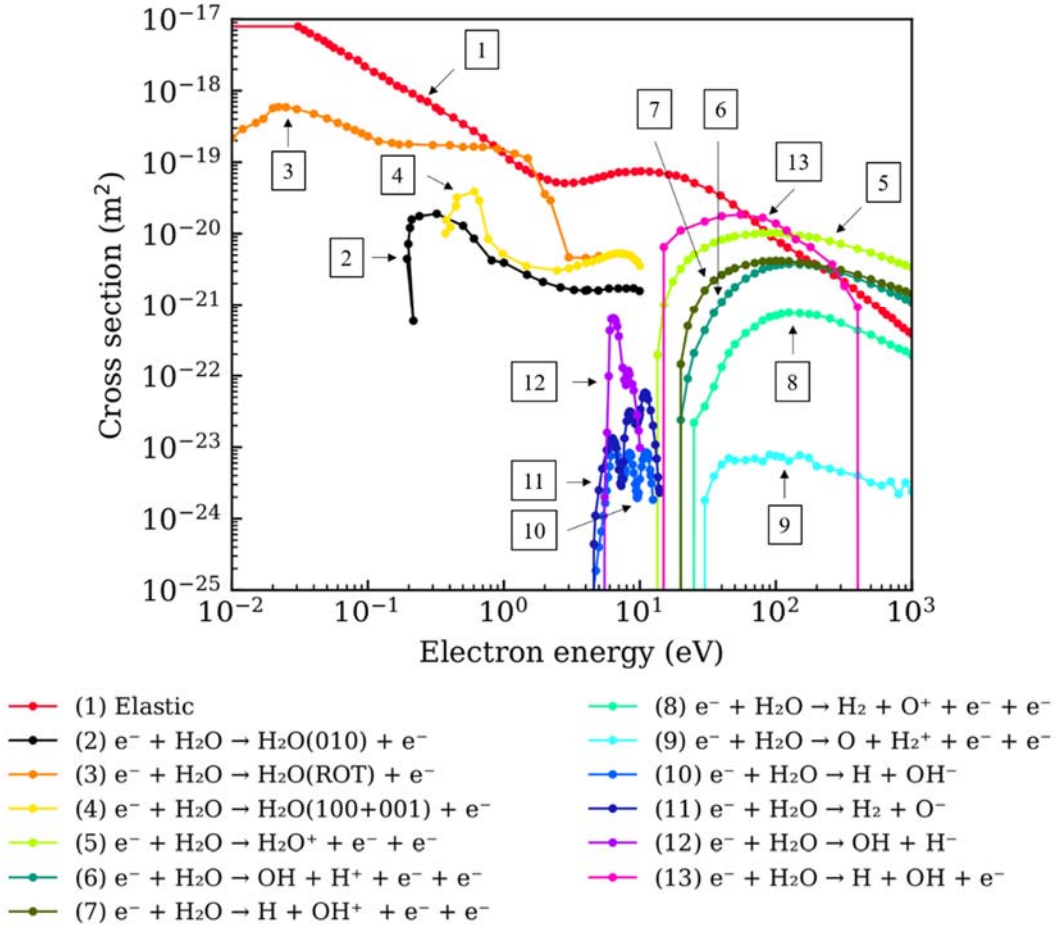

Figure 2. H_2O cross section set created in this work.

2.2. THE 0D MODEL

(a) Model description

The calculations were performed by the Fortran 90-model, ZDPlasKin (Zero-Dimensional Plasma Kinetics solver).[22] This is a zero-dimensional model and, as a result, the plasma is assumed to be homogeneous. The changes in concentration will only be a function of time. Therefore, only the mass conservation equation for every species, the Boltzmann equation and the gas thermal balance is solved. Thus, ZDPlasKin follows the time evolution of species densities and gas temperature. The mass conservation equation for every species is written as follows:

$$\frac{dn_s}{dt} = \sum_{j=1}^{j_{max}} Q_{sj} = \sum_{j=1}^{j_{max}} R_j\left[a_{sj}^R - a_{sj}^L\right], \quad (1)$$

$$R_j = k_j \prod_l n_l, \quad (2)$$

where n_s is the density of the species s, Q_{sj} is the source term for reaction j of the species s, a_{sj}^R and a_{sj}^L represent the stoichiometric coefficients on the right and left side, respectively, of species s for reaction j. R_j is the reaction rate and k_j the reaction rate coefficient.

As the chemical reactions produce or consume energy, and energy is transferred from the electrons to the gas, the model also self-consistently calculates the gas temperature as a function of time:[6]

$$N\frac{\gamma k_B}{\gamma-1}\frac{dT_{gas}}{dt} = P_{el} - \sum_{j=1}^{j_{max}} \Delta H_j * R_j - P_{ext}, \quad (3)$$

where N is the total gas density, and γ is the specific gas heat ratio. P_{el} is the power transferred from the electrons to the heavy particles as a consequence of elastic collisions and ΔH_j the enthalpy released or consumed during reaction j. In addition, cooling due to heat conduction is accounted for by assuming a parabolic radial profile, that can be calculated as [6]

$$P_{ext} = \frac{8\lambda}{R^2}\left(T_{gas} - T_{wall}\right), \quad (4)$$

$$\lambda = \left(0.071T_{gas} - 2.33\right) * 10^{-5}, \quad (5)$$

where λ (W cm^{-1} K^{-1}) is the thermal gas conductivity of CO_2 and R the tube radius (taken as 0.7 cm in this work).[6]

The model follows a volume moving through a cylindrical tube in a microwave (MW) discharge, consisting of a plasma region as well as an afterglow. As a result of the 0D model, all variables are taken as uniform in the radial direction, and diffusion and heat conduction are neglected along the reactor axis. However, by using the gas flow velocity, the time-dependence of the 0D model can be converted into an axial spatial dependence, thus creating a pseudo-1D model. This allows for describing the variations of species densities and gas temperature along the reactor axis (z). [19] Using the conservation of mass flow rate, the velocity *v* of a volume in the tube can be calculated:

$$v = \frac{Q_m}{\rho * A} = \frac{Q_m}{\sum_s n_s M_s * \pi R^2}, \quad (6)$$

where Q_m is the mass flow rate, ρ is the mass density (calculated for each species from the number density n and the mass M), and A is the cross section area. To describe a MW plasma, with power input through a waveguide, a triangular power density profile is incorporated, described by: [19]

$$Q_{MW}(z) = \left(1 - \left|\frac{z-(z_p+L/2)}{L/2}\right|\right) * P_{max} \; if \; z_p \le z \le z_p + L \quad (7)$$

$$P_{MW} = A\int_{z_p}^{z_p+L} Q_{MW}(z)dz = \frac{AL}{2}Q_{max} \quad (8)$$

In any other case, the axial coordinate is outside the plasma, and thus Q_{MW} is zero. In the formula, z_p is the beginning of the plasma, and L the length of the plasma (figure 3). Using $Q_{MW,}$ the total deposited power P_{MW} can be calculated, where Q_{max} is the maximum power deposition density. If divided by two, the latter also gives the mean power deposition density.

The calculations are performed for an initial temperature of 300 K, a pressure of 300 mbar and a maximum power deposition density 100 W/cm^3. The temperature rises during the calculation, as indicated above. It reaches a maximum (in case of pure CO_2) up to 3000 K, as shown in the results section. The specific energy input (SEI) is an input in the model as well, using a value of 2 eV/molecule, and can be used to calculate the power and plasma length:

$$SEI = \frac{P_{MW}\, T_{ref}\, k_b * 60}{\Phi\, p_{ref}\, e\, 10^{-6}}, \tag{9}$$

where Φ represents the gas flow rate in sccm (in the model we take a constant value of 5000 sccm), T_{ref} and p_{ref} are the reference temperature (273.15 K) and pressure (10^5 Pa). The rest are conversion factors, in which *e* represents the elementary charge used as a conversion factor from J to eV, 10^{-6} is the conversion factor from cubic centimetre to cubic metre, and 60 from minutes to seconds.

The 0D ZDPlasKin model is supported by the use of a Boltzmann solver, Bolsig+, for calculating the Boltzmann equation for electrons in weakly ionised gases in uniform electric fields. It uses a two-term approximation to obtain the electron energy distribution function (EEDF) from the provided cross sections.

Note that ZdPlasKin uses Bolsig+ that does not solve the Boltzmann equation time-dependently, but assumes a steady-state solution. In other words, the Electron Energy Distribution Function (EEDF) is assumed to be determined by the instantaneous value of the reduced electric field. The Boltzmann solver is called when significant changes occur in the plasma. The significance of changes is dependent on the relative tolerance, which in these calculations is 10^{-5}. Therefore a total change smaller than this tolerance will not be seen as significant, which allows the code to work more efficiently. This approach is considered sufficient in most of the simulation, apart from the regions of a sudden change of E/N, e.g. when the plasma is turned on and off. Furthermore, the time step in the simulations is taken smaller during the plasma-on time. Due to the changes that occur, the Boltzmann solver is then called every time-step in the plasma, being every 10^{-10} s. Based on previous experience, this was found to be sufficient to take into account the evolution of the plasma composition.

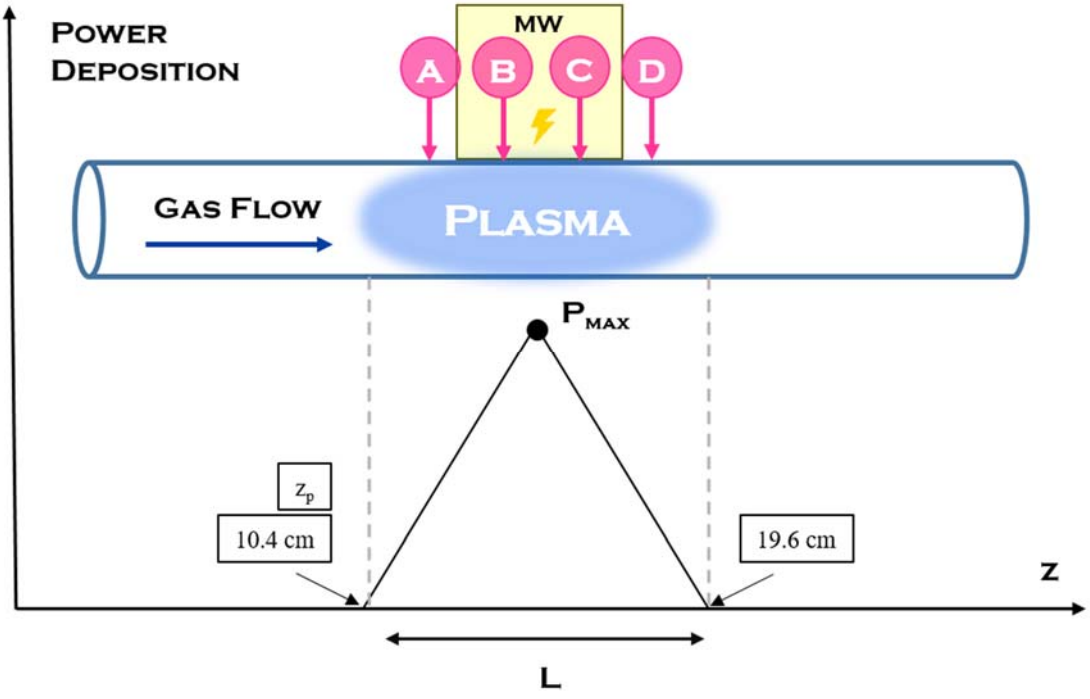

Figure 3 Schematic overview of the reactor geometry and the deposited power, considered in the model. L represents the plasma length. The meaning of A, B, C, D is used in the results section.

(b) Chemistry set

As a basis for the creation of the CO_2/H_2O set, we used the pure CO_2 set of Vermeiren and Bogaerts.[47] In this model, all vibrational asymmetric mode levels up to the dissociation energy of CO_2 (5.5 eV) are included, corresponding to all (0 0 v) levels up to (0 0 21), represented by V_1-V_{21}.[6,7,19,47] This is to account for the fact that the asymmetric mode plays an essential role in de CO_2 dissociation, as a result of the vibrational-vibrational (VV) exchanges between molecules, the so-called ladder climbing.[1] The VV exchanges lead to higher populations of higher vibrational levels, whereas in vibrational-translational (VT) exchanges, the energy of the vibrational modes is lost to translations, so the vibrational levels get more easily depopulated. For the other two modes (symmetric stretching and bending), only the lower-lying levels are included (represented here by V_a-V_d).[6,7,19,47] Given the Fermi resonance between some ν_1 and ν_2 modes, the four lowest-lying levels of the bending mode are included, and so by implication also the resonant symmetric stretching mode levels. For CO and O_2, we take into account ten and four vibrational levels, respectively. Note that superelastic collisions are included, as they do affect the EEDF.[5,48]

Note that our model focuses on the CO_2 vibrational levels in the asymmetric mode, up to the dissociation limit, while it only accounts for four effective symmetric mode levels.[7] This is different from the model of Silva et al., which includes many more symmetric mode levels and a detailed description of the bottom of the vibrational ladder, but does not account for the asymmetric mode levels up to the dissociation limit.[49] Here, we chose the approach of all asymmetric mode levels, to show the effect of H_2O addition on the entire VDF of the asymmetric mode. Future work will focus on the comparison and combination of both models, to account for a comprehensive description of both asymmetric and symmetric/bending vibrational mode levels.

The H_2O-related reactions added to this model, include (i) electron impact reactions with H_2O (cf. the cross section set in section 2.1), (ii) VT-reactions associated with the quenching of vibrationally excited CO_2 levels by H_2O, and (iii) the chemistry associated with CO_2 and H_2O. Because of the high vibrational self-relaxation rates in H_2O (orders of magnitude faster than relaxation by collisions with other molecules)[50] and the lack of available data, no VV reactions of H_2O(-CO_2) were considered. As a consequence, no internal structure of H_2O was included. The species included in the model are listed in table 1, with the ones in italic representing the new species added to the previous CO_2 model.

As this paper focusses on the addition of H_2O on the VDF of CO_2, the chemistry set in our model does not include all possible species or reactions, e.g., it excludes water clusters, H^+ and H_3^+, as well as electron impact reactions and ion kinetics and V-T kinetics of species with lower densities, such as OH, H_2 and hydrocarbons. The main reason is indeed the low concentrations of these species, e.g., the H_2 density is 100 times lower than the H_2O density, and the densities of hydrocarbons are 10^{10} to 10^{12} times lower, as these species originate from the already low concentrations of H_2O. To accommodate for the lack of V-T rate coefficients of CO_2(v) with these neutral species, we used a general V-T rate coefficient for the various neutral species.

Note that our model does not include wall reactions, such as recombination to form other species. This will affect our plasma species densities to some extent, so the absolute values have to be considered with caution. On the other hand, the simulations are rather generic, and not specific for a certain plasma set-up. It should be realised that surface recombination is generally quite material-dependent and temperature-dependent, which would narrow the applicability of our results. Note that our results should apply to a rather large plasma tube, or when the plasma is concentrated in the centre and does not reach the walls

Table 1: Species included in the model for the CO_2/H_2O MW plasma

Neutral ground state species
CO_2, CO, O_2, O, C
H_2O, O_3, OH, H, H_2, CH_2, HO_2, H_2O_2, CH, CH_3, CH_2OH, CH_2O, CH_3OH, CH_3O, HCO
Charged species
CO_2^+, CO^+, CO_4^+, O^-, O_2^-, CO_3^-, CO_4^-, e^-
H_2O^+, OH^-, OH^+, H_2^+, H_3O^+, O^+, O_2^+, O_3^-

Excited Species

$O_2[V_1\text{-}V_4]$, $CO[V_1\text{-}V_{10}]$, $CO_2[V_1\text{-}V_{21}]$, $CO_2[V_a\text{-}V_d]$, $CO_2[E_1]$, $O_2[E_{1\text{-}5}]$, $CO[E_{1\text{-}6}]$

The VT CO_2/H_2O reaction rate coefficients are calculated with the following expression:[51]

$$k = \frac{1}{N_A} \exp\left[A + BT^{1/3} + CT^{2/3}\right], \quad (10)$$

where A, B, and C are fitting constants, and N_A is Avogadro's number, used in order to express the rate coefficients in units of $cm^3 \cdot s^{-1}$. The VT-reactions and rate coefficients for the (lower) symmetric and asymmetric levels (the higher levels of the latter will be scaled, see below) were obtained from Blauer[51] and are listed in Appendix 1 (A1). In general, the reactions for the vibrational levels of the asymmetric stretch mode can be summarised as:

1. $CO_2(00^0v) + H_2O \rightarrow CO_2(01^1(v\text{-}1)) + H_2O \quad (k_1)$
2. $CO_2(00^0v) + H_2O \rightarrow CO_2(10^0(v\text{-}1)) + H_2O \quad (k_2)$
3. $CO_2(00^0v) + H_2O \rightarrow CO_2(11^1(v\text{-}1)) + H_2O \quad (k_3)$

Since the resulting levels, produced by these reactions 1, 2 and 3, are assumed to be depopulated quickly through further VT-relaxation, we can simply assume them to be in thermal equilibrium with the asymmetric levels, and thus we can simply write the following reaction for v > 1:[7]

$$CO_2(00^0v) + H_2O \rightarrow CO_2(00^0(v\text{-}1)) + H_2O \quad (11)$$

The resulting rate coefficient is then given by $k_{total} = k_1 + k_2 + k_3$.

Note that all the presented rate coefficients correspond to forward processes. For the reverse reaction rate coefficients k', we use detailed balance, according to:

$$k'_{reverse} = k_{forward} * exp\left(-\frac{\Delta H}{k_b T}\right), \quad (12)$$

where ΔH is the enthalpy released/absorbed during the reaction, k_b the Boltzmann constant and T the temperature.

For the scaling of the rate coefficients listed in Appendix (A1) towards the higher levels, the method of Schwartz, Slawsky, and Herzfeld, i.e., the SSH theory, was used.[7,52] The SSH theory is part of the first-order perturbation theories (FOPT) and can provide relatively simple expressions for the state-specific relaxation rate coefficients. The assumption made here is that strong, short-range, repulsive forces are effective in producing vibrational transitions. However, one needs to be cautious when using the SSH theory for high temperatures or quantum levels, because it is known to overestimate the vibrational transition probabilities in those cases.[49] As we apply it to temperatures up to 3000 K (see below), the values might indeed be unrealistically high. Nevertheless, in order to better compare the influence of H_2O on the CO_2 vibrational kinetics with existing calculations,[5,6] we decided here to keep the same formulation as in previous works and we implement the SSH theory as well for the new CO_2-H_2O reactions. Alternatives approaches could be to try to adapt the Forced Harmonic Oscillator Theory (FHO Therory)[53] to the case of CO_2 or to impose an upper bound to the V-T and V-V rate coefficients, as it is done in Silva et al.[54]

The same scaling strategy for CO_2-H_2O VT-reactions was used as applied by Kozák and Bogaerts for the pure CO_2 model:[7]

$$k_{n,n-1} = k_{1,0} Z_n \frac{F(\gamma_n)}{F(\gamma_1)}, \quad (13)$$

where *n* is the vibrational level of the molecule, in this case, the asymmetric vibrational level of CO_2, noted as (0 0 v) = (0 0 n), $k_{n,n-1}$ is the rate constant for VT-relaxation from (0 0 n) to (0 0 (n-1)), and therefore $k_{1,0}$ represents the basic rate constant for (0 0 1) to (0 0 0), and Z_n is the scaling factor (see details in previous work).[6] Note that this formula is applied to the 21 asymmetric mode vibrational levels included in this model, since for the symmetric and bending mode only the lower levels were included, and no scaling was needed.

Furthermore, the function $F(\gamma_n)$ in equation (13) is given by:

$$F(\gamma_n) = \frac{1}{2}\left[3 - exp\left(-\frac{2}{3}\gamma_n\right)\right] exp\left(-\frac{2}{3}\gamma_n\right), \quad (14)$$

$$\gamma_n = \frac{0.32\Delta E}{\alpha}\left(\frac{\mu}{T_g}\right)^{1/2}, \quad (15)$$

where the parameter γ_n is a measure of the adiabaticity (the amount of energy transferred). To calculate this parameter, the reduced mass $\mu = {m_1 m_2}/{m_1 + m_2}$ of the colliding species, and the value of the parameter for the exponential repulsive potential between the colliding species α, are needed. α can be calculated through:

$$\alpha = \frac{17.5}{r_0}, \quad (16)$$

where r_0 is the distance at which the Lennard-Jones potential is zero. In the case of CO_2-H_2O VT-collisions, r_0 is 3.60 Å.[55]

In figure 4, we compare the rate coefficients of the CO_2-H_2O VT-relaxation collisions (i.e., the above mentioned k_{total}) with those of the corresponding CO_2-CO_2 VT-relaxation, for all vibrational levels of the asymmetric mode. It can be seen that at 300 K the CO_2-H_2O VT-relaxation has overall higher reaction rate coefficients, even by several orders of magnitude. This indicates that the H_2O molecules will be more effective than the CO_2 molecules in quenching the CO_2 asymmetric vibrational-mode levels. However, this behaviour is only valid up to a gas temperature of around 1700 K. Indeed, for higher gas temperature, the CO_2-CO_2 VT-relaxation has higher rate coefficients than the CO_2-H_2O VT-relaxation. Therefore, we expect that the addition of H_2O will result in a lower population of the CO_2 vibrational levels through VT-relaxation for gas temperatures below 1700 K, while at higher temperatures, the addition of H_2O might have a positive effect on the CO_2 vibrational levels. The impact of this process on the CO_2 vibrational distribution function (VDF) is investigated below.

Besides the H_2O cross section set, described in section 2.1, and the CO_2-H_2O VT-reactions, also some other CO_2-H_2O chemical reactions were added in the model. This chemistry can be found in Appendix 3 (A3).

Note that the present MW results were not compared with experiments, so the results must be considered with caution, and essentially as describing general qualitative trends. However, although the model has not been validated for the conditions under study, the CO_2 set used in this work was used in previous publications, where comparisons with experimental results in gliding arc plasma[8,13,56–58], and in dielectric barrier discharges (DBD)[59,60] were performed, while CO_2/H_2O chemistry was used and extensively compared with experiments in DBD plasmas.[14,61]

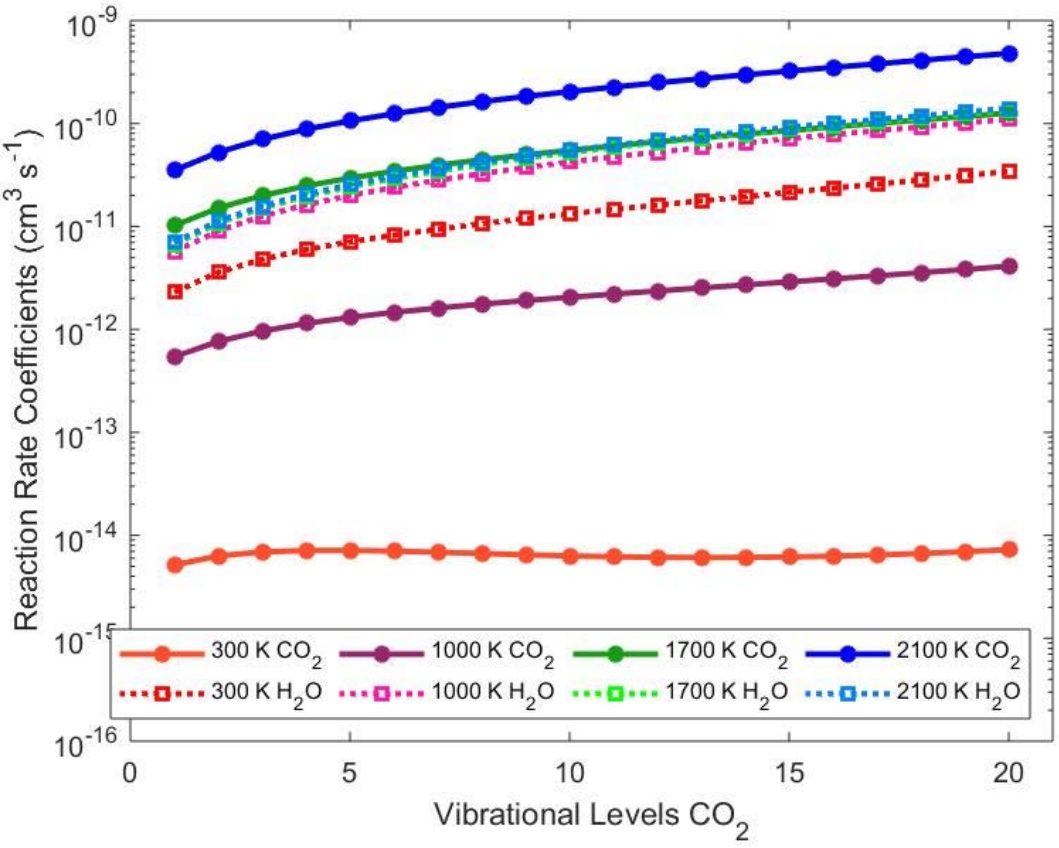

Figure 4 Scaled rate coefficients of the quenching of the CO_2 asymmetric vibrational mode levels by CO_2 and H_2O (squares/solid lines and diamonds/dashed lines, respectively). The H_2O rate coefficients are higher (up to several orders of magnitude) than the ones for CO_2 at temperatures up to 1700 K, while for higher temperatures, H_2O shows a lower quenching effect than CO_2.

3. RESULTS AND DISCUSSION

As mentioned before, the purpose of this paper is to obtain an understanding of how H_2O influences the CO_2 asymmetric mode vibrational levels, because of their important role in CO_2 dissociation. Therefore, we plot in figure 5 the normalised vibrational distribution functions (VDFs) of the asymmetric mode vibrational levels, for pure CO_2 and with the addition 10% H_2O, at four different positions in the plasma (see figure 3; the plasma runs from 10.4 cm to 19.6 cm). The corresponding results for 20% H_2O can be found in the Appendix (A4.1). We want to study the separate influence of the electron impact reactions of H_2O (affecting the EEDF, and thus the rates of electron-impact vibrational excitation), and of the CO_2-H_2O VT-reactions. For this purpose, the electron impact reactions of H_2O were added separately to the model, as well as the VT-reactions. In the end, the VDF was calculated with the full set, including both electron impact and VT-reactions.

Three observations can be made when looking at figure 5. First, the addition of H_2O leads to a longer time needed for thermalisation. Indeed, while in the pure CO_2 case, the VDF is thermalised already at 16.21 cm (figure 5C), upon H_2O addition, the VDF is not even fully thermalised at the end of the plasma (figure 5D), exhibiting deviations from the Boltzmann distribution. However, when only the VT-reactions of H_2O are added, the thermalisation follows the same trend as for pure CO_2. This hints toward the role of the gas temperature, as it reaches higher values in these two cases (see figure 6(B) below). As can be seen in figure 4, with increasing temperature, the VT-rate coefficients increase, leading to faster thermalisation of the VDFs.

The second observation is that the addition of only the H_2O electron impact reactions already leads to a smaller population of the lower vibrational levels of CO_2, while for the higher vibrational levels ($v > 16$), the differences are less apparent. The reasons for this are discussed below.

Most importantly, the modifications in the VDF seem most prominent upon addition of the electron impact reactions with H_2O, while the effect of the VT-relaxations looks minor. This is somewhat unexpected since it is typically emphasised that H_2O has a significant quenching character through the VT-relaxation.[1]

To explain the influence of the electron impact reactions with H_2O on the VDF, we need to look at the gas and electron temperatures and the electron density in the plasma.

As can be deduced from figure 6(A), the addition of H_2O leads to a higher electron temperature. This is explained by the electron density being almost a factor three lower upon addition of H_2O (figure 6(B)). The lower electron density is a consequence of the strong electron attachment with H_2O. Based on the reaction rates calculated in our model, the ratio of electron attachment to electron ionisation is indeed almost 40% higher for the combined CO_2-H_2O system than for pure CO_2. Furthermore, the reduction of the attachment rate of H_2O to 10% of the original value leads to a doubling of the electron density compared to the initial electron density of the CO_2/10% H_2O mixture (Appendix A4 figure 4.3 confirming the crucial role of dissociative electron attachment to H_2O in the overall kinetics).

On the other hand, the addition of H_2O leads to a lower gas temperature (figure 6(C)). H_2O is known to have a high specific heat capacity (i.e., 2.842 kJ/(kg K) vs 1.371 kJ/ (kg K) for CO_2 at 2000 K)[62] and will, therefore, need to take up more energy before heating up. The drop in gas temperature will not only cause the reaction rates, in general, to be lower, as they are a function of the gas temperature but in addition, it causes that the reaction rates of VT-CO_2-H_2O relaxation will be slightly higher than for pure CO_2 (see figure 4). Therefore, the change in gas temperature may provide an explanation for the difference in VDF. To verify this effect, the gas temperature profile of pure CO_2 was implemented in the CO_2-H_2O runs. The result can be found in Appendix A4 In general, it can be said that the gas temperature influences thermalisation. However, due to the higher gas temperature, the thermalisation will occur faster in pure CO_2 as well; and therefore, the change of gas temperature alone is not able to explain the changes in the VDF; even more, in general, the effect is quite minimal (see figure A4.4 in Appendix A4).

If looked at it differently, quenching of vibrational levels is often related to the V-T reactions. Therefore, we reduced those to half; however, the reduction did not lead to any significant changes.

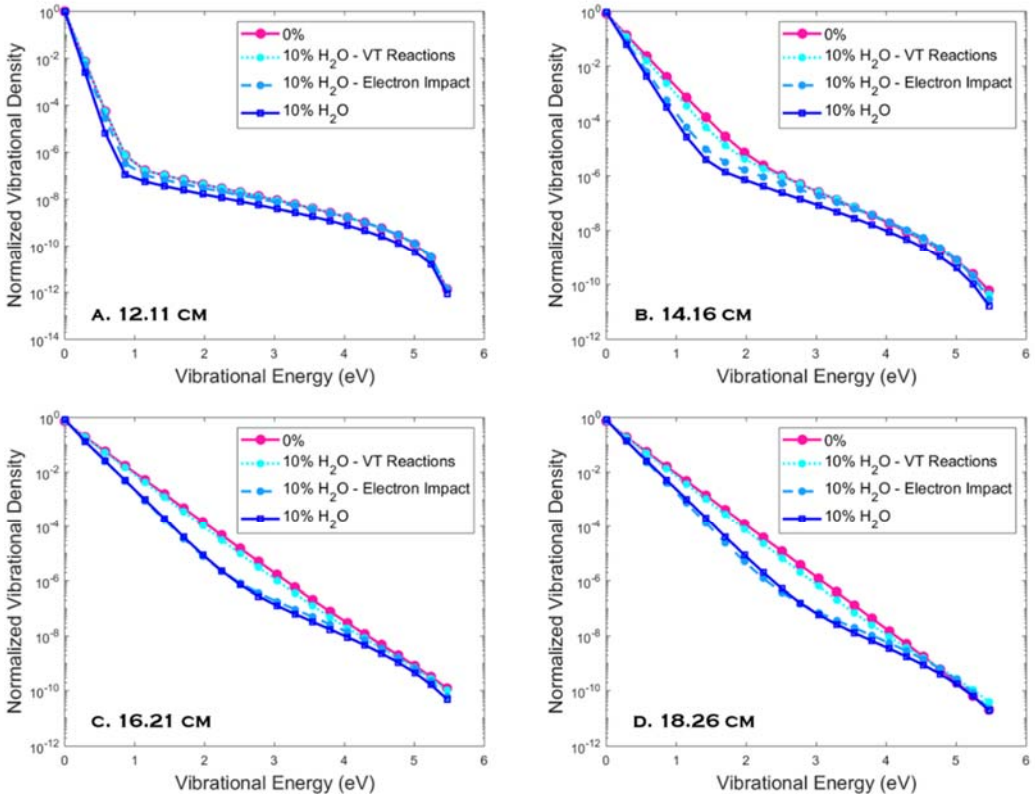

Figure 5 Calculated VDFs in pure CO_2, and upon 10% H_2O addition, at four different positions in the plasma tube (see figure 3), when only the VT-reactions with H_2O are included (dotted lines), when only electron impact reactions with H_2O are added (dashed lines), and when both processes are included (full lines).

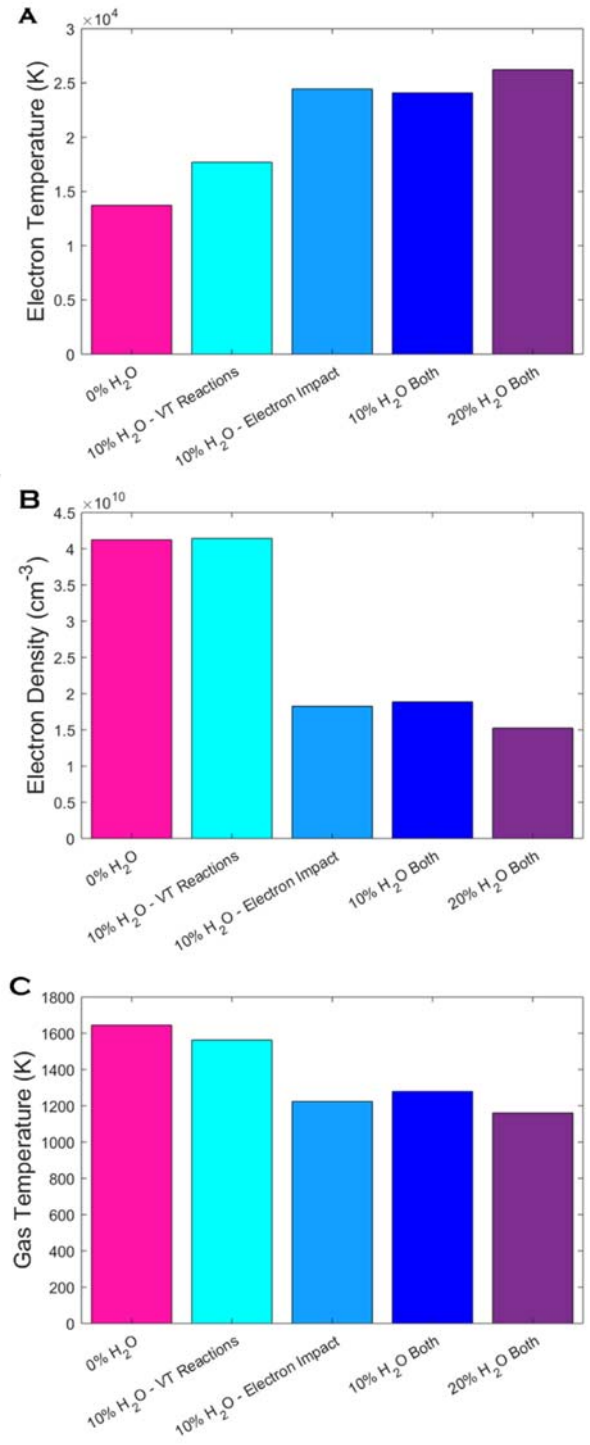

As the gas temperature (and VT-relaxation) does not seem to play a big role at the conditions under study, we have to look in more detail how the changes in electron temperature and electron density will affect the CO_2 VDFs.

The higher electron temperature (figure 6(A)) will cause more electron impact excitation to the higher asymmetric-mode vibrational levels, but less excitation to the lower vibrational levels. This is indeed illustrated in the Appendix (A4; figure A4.5), showing a drop in electron impact vibrational excitation rate for the asymmetric mode levels up to v=16, but a slight rise for levels v ≥ 17. The latter is also confirmed from figure 7, showing the distribution of electron energy towards different vibrational levels of the asymmetric stretch mode of CO_2, as a function of the mean electron energy. It is indeed clear that at higher electron energy/temperature, the higher vibrational levels are gradually more populated.

This shift in electron impact excitation from lower to higher vibrational levels, due to the higher electron temperature, can explain why H_2O addition goes in line with a smaller population of the lower CO_2 vibrational levels upon H_2O addition but has only a small influence on the population of the higher vibrational levels. However, this effect is rather small and, like the influence of the gas temperature, cannot justify the observed effect in the VDFs.

The decrease in electron density (figure 6(B)) will cause a reduction in electron impact excitation by reducing the input of energy into the excited vibrational states. To evaluate this effect, we decreased in the model the rates of all e-V processes to half their original values in pure CO_2, which causes a decrease in the VDF similar to the effect H_2O has on the VDFs, as can be seen in figure 8. Therefore, this gives a strong indication of the importance of the electron impact reactions and the effect of H_2O on the electron density, and thereby affecting the electron impact reactions.

Thus, the present results highlight the importance of the electrons and the electron kinetics in CO_2-H_2O mixtures.

Figure 6 Calculated overall average electron temperature (A), electron density (B), and gas temperature (C) for pure CO_2 and upon addition of 10 and 20% H_2O. For 10% H_2O, the results are also plotted when only the VT-reactions and only the electron impact reactions with H_2O are added, to illustrate their separate effect. Adding H_2O leads to a higher electron temperature, lower electron density, and lower gas temperature. The VT-relaxation slightly reduces the effect, but only to a minor extent, showing the dominant effect of the electron impact reactions with H_2O.

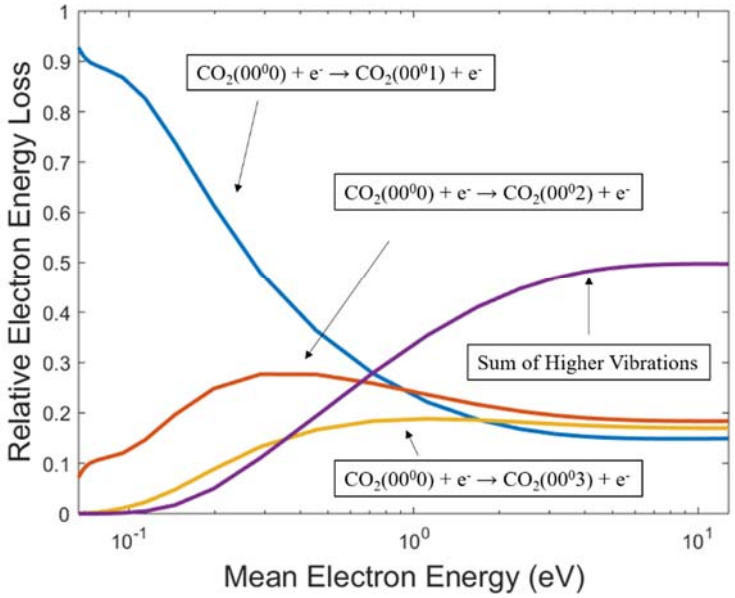

Figure 7 Fraction of electron energy transferred to different vibrational levels of the asymmetric stretch mode, as a function of the mean electron energy, showing the shift towards higher levels upon higher mean electron energy.

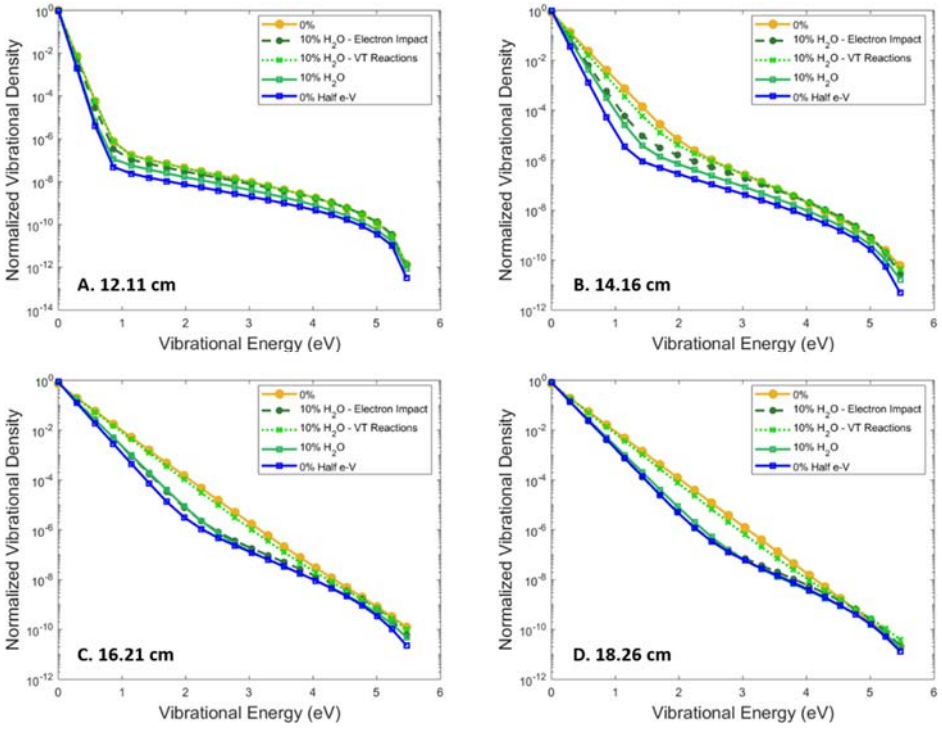

Figure 8 Calculated VDFs in pure CO_2 (with the original rates, as well as the electron impact excitation rates reduced to half) and upon 10% H_2O addition (as in Figure 5). By decreasing the electron impact excitation rates to half the original values, the VDF becomes similar to the effect of H_2O addition, indicating that the reduced electron density upon H_2O addition is the dominant factor for explaining the influence of H_2O addition.

Finally, we performed calculations for a broader range of conditions, to evaluate how these parameters affect the VDFs. In general, our calculations reveal that the presence of H_2O is the determining factor, within the parameter range investigated. When increasing the H_2O concentration, the changes in the VDF, as well as in the electron density (lower), temperature (higher) and the gas temperature (lower), become more apparent, as illustrated in the Appendix (Figure A.4.1 and Figure A.4.6) and Figure 6 above. The reduction of H_2O concentration has the opposite effect. The power density shows only a minimal change, within the range investigated. Note that in this study we use the SEI as an input, as well as the power density, based on which the plasma length is determined. An increase in SEI leads to extra energy in the system, which leads to a higher electron and gas temperature as well as higher electron densities. This will result in more electron impact reactions, which are more important for the lower levels and therefore we observe a minor increase in the densities of the lower-lying levels, while a lower SEI will have the opposite effect.

CONCLUSION

We performed a chemical kinetics modelling study to obtain insight into the vibrational kinetics of a CO_2/H_2O mixture. More specifically, we studied the effect of adding H_2O to a CO_2 MW plasma on the VDF of the CO_2 asymmetric mode levels. As a first important step, we created a cross section set for H_2O electron impact reactions, using a swarm-based method and an extensive literature study. This resulted in a new cross section set containing 13 reactions, i.e., elastic momentum transfer, three attachment, five ionisation, and four excitation cross sections. Subsequently, we developed a 0D chemical kinetics model for a CO_2-H_2O mixture, including this new cross section set, as well as CO_2-H_2O VT-relaxation and other relevant CO_2-H_2O chemistry. We used this model to calculate the VDF of the CO_2 asymmetric mode vibrational levels, for pure CO_2, 10% and 20% of H_2O addition.

The results showed an overall decrease in densities of the vibrational levels, mainly for the lower levels, corresponding to a lower "effective vibrational temperature". The dominant effect was shown to be the significant decrease of the electron density upon addition of H_2O, as a result of the strong dissociative attachment with H_2O molecules. This lower electron density translates into a smaller input of energy into the vibrational manifold, as the e-V rate coefficients are not very sensitive to the "electron temperature" in the relevant range for this study and, accordingly, the lower electron density results in a smaller degree of vibrational excitation. The colder gas temperature with H_2O and the higher electron temperature also contribute to the effect, although in a smaller extent, by modifying the V-T rate coefficients and facilitating the direct excitation of the higher vibrational levels, respectively.

The present results demonstrate the importance of the electron kinetics in this system. Thus, the overall message here is that, at the conditions under study, the H_2O-CO_2 VT-reactions will not play a significant role in quenching of the CO_2 vibrational levels, in contrast to what is commonly assumed,[1] therefore, opening a new possibility for further research into this system.

ACKNOWLEDGEMENTS

This research was supported by FWO – PhD fellowship-aspirant, Grant 1184820N. VG and TS were partially supported by the Portuguese FCT, under Project Nos. UID/FIS/50010/2019

REFERENCES

(1) Snoeckx, R.; Bogaerts, A. *Chem. Soc. Rev.* **2017**, *46*, 5805–5863.

(2) Asisov, R. I.; Vakar, A. K.; Jivotov, V. K.; Krotov, M. F.; Zinoviev, O. A.; Potapkin, B. V; Rusanov, A. A.; Rusanov, V. D.; Fridman, A. A. *Proc. USSR Acad. Sci.* **1982**, *271* (1).

(3) Kochetov, I. V.; Pevgov, V. G.; Polak, L. S.; Slovetsky, D. I. *Plasma Chemical Processes*; Nauka: Moscow, 1979.

(4) Rusanov, V. D.; Fridman, A. A.; Sholin, G. V. *Sov. Phys. Uspekhi* **1981**, *24* (6), 447.

(5) Pietanza, L. D.; Colonna, G.; Ammando, G. D.; Laricchiuta, A.; Capitelli, M. *Plasma Sources Sci. Technol.* **2015**, *24* (4).

(6) Kozák, T.; Bogaerts, A. *Plasma Sources Sci. Technol.* **2014**, *24* (1), 015024.

(7) Kozàk, T.; Bogaerts, A. *Plasma Sources Sci. Technol.* **2014**, *23* (4), 045004.

(8) Ramakers, M.; Heijkers, S.; Tytgat, T.; Lenaerts, S.; Bogaerts, A. *J. CO2 Utlization* **2019**, *33* (March 2019),

121–130.

(9) Heijkers, S.; Snoeckx, R.; Kozák, T.; Silva, T.; Godfroid, T.; Britun, N.; Snyders, R.; Bogaerts, A. *J. Phys. Chem. C* **2015**, *119* (23), 12815–12828.

(10) Snoeckx, R.; Wesenbeeck, K. Van; Lenaerts, S.; Cha, M. S. *Sustain. Energy Fuels* **2019**, *3*, 1388–1395.

(11) Terraz, L.; Silva, T.; Morillo-Candas, A.; Guaitella, O.; Tejero-del-Caz, A.; Alves, L. L.; Guerra, V. *J. Phys. D. Appl. Phys.* **2020**, *53*.

(12) de la Fuente, J. F.; Moreno, S. H.; Stankiewicz, A. I.; Stefanidis, G. D. *Int. J. Hydrogen Energy* **2016**, *41* (46), 21067–21077.

(13) Cleiren, E.; Heijkers, S.; Ramakers, M.; Bogaerts, A. *ChemSusChem* **2017**, *10*.

(14) Snoeckx, R.; Ozkan, A.; Reniers, F.; Bogaerts, A. *ChemSusChem* **2017**, *10* (2), 409–424.

(15) Indarto, A.; Yang, D. R.; Choi, J. W.; Lee, H.; Song, H. K. *J. Hazard. Mater.* **2007**, *146* (1–2), 309–315.

(16) Nunnally, T.; Gutsol, K.; Rabinovich, A.; Fridman, A.; Gutsol, A.; Kemoun, A. *J. Phys. D. Appl. Phys.* **2011**, *44* (27).

(17) Chen, G.; Godfroid, T.; Britun, N.; Georgieva, V.; Delplancke-Ogletree, M. P.; Snyders, R. *Appl. Catal. B Environ.* **2017**, *214*, 114–125.

(18) Ihara, Ouro, Ochiai, I. *Bull. Chem. Soc. Jpn* **1996**, *69*, 241–244.

(19) Berthelot, A.; Bogaerts, A. *J. Phys. Chem. C* **2017**, *121* (15), 8236–8251.

(20) Grofulović, M.; Alves, L. L.; Guerra, V. *J. Phys. D. Appl. Phys.* **2016**, *49* (39).

(21) Hagelaar, G. J. M.; Pitchford, L. C. *Plasma Sources Sci. Technol.* **2005**, *14* (4), 722–733.

(22) Pancheshnyi, S.; Eismann, B.; Hagelaar, G. J. M.; Pitchford, L. C. University of Toulouse, LAPLACE, CNRS-UPS-INP: Toulouse 2008.

(23) Petrović, Z. L.; Šuvakov, M.; Nikitović, Z.; Dujko, S.; Šaić, O.; Jovanović, J.; Malović, G.; Stojanović, V. *Plasma Sources Sci. Technol.* **2007**, *16* (1).

(24) LXCat www.lxcat.net.

(25) Hasegawa, H.; Date, H.; Shimozuma, M. *J. Phys. D. Appl. Phys.* **2007**, *40* (8), 2495–2498.

(26) Petrović, Z. L.; Dujko, S.; Marić, D.; Malović, G.; Nikitović, Ž.; Šašić, O.; Jovanović, J.; Stojanović, V.; Radmilović-Radenović, M. *J. Phys. D. Appl. Phys.* **2009**, *42* (19).

(27) TRINITI database www.lxcat.net/TRINITI.

(28) Itikawa, Y.; Mason, N. *J. Phys. Chem. Ref. Data* **2005**, *34* (1), 1–22.

(29) Hayashi, M.; Pitchford, L. C.; McKoy, B. V.; Chutjian, A.; Trajmar, S. *Swarm Studies and Inelastic Electron-Molecule Collisions*; Springer-Verslag: New York, 1987.

(30) Morgan. Morgan Database www.lxcat.net/Morgan.

(31) Phelps Database www.lxcat.net/Phelps.

(32) Ness, K. F.; Robson, R. E.; Brunger, M. J.; White, R. D. *J. Chem. Phys.* **2012**, *136* (2).

(33) Muñoz, A.; Blanco, F.; Garcia, G.; Thorn, P. A.; Brunger, M. J.; Sullivan, J. P.; Buckman, S. J. *Int. J. Mass Spectrom.* **2008**, *277* (1–3), 175–179.

(34) Ness, K. F.; Robson, R. E. *Phys. Rev. A* **1988**, *38* (3), 1446–1456.

(35) Satoru Kawaguchi; Takahashi, K.; Satoh, K.; Itoh, H. *Jpn. J. Appl. Phys.* **2016**, *55*, 07LD03.

(36) Gianturco, F. A.; Thompson, D. G. *J. Phys. B. Atom. Molec. Phys.* **1980**, *13*, 613–625.

(37) Yousfi, M.; Benabdessadok, M. D. *J. Appl. Phys.* **1996**, *80* (12), 6619–6630.

(38) Faure, A.; Gorfinkiel, J. D.; Tennyson, J. *Mon. Not. R. Astron. Soc.* **2004**, *333*, 323–333.

(39) Jung, K.; Antoni, T.; Muller, R.; Kochem, K.; Ehrhardt, H. *J. Phys. B At. Mol.phys* **1982**, *15*, 3535–3555.

(40) MacHado, L. E.; Brescansin, L. M.; Iga, I.; Lee, M. T. *Eur. Phys. J. D* **2005**, *33* (2), 193–199.

(41) Cho, H.; Park, Y. S.; Tanaka, H.; Buckman, S. J. *J. Phys. B At. Mol. Opt. Phys.* **2004**, *37* (3), 625–634.

(42) Itikawa, Y. *Journal of the Physical Society of Japan*. 1972, pp 217–226.

(43) Makochekanwa, C.; Kajita, R.; Kato, H.; Kitajima, M.; Cho, H.; Kimura, M.; Tanaka, H. *J. Chem. Phys.* **2005**, *122* (1).

(44) Joshipura, K. N.; Pandya, S. H.; Mason, N. J. *Eur. Phys. J. D* **2017**, *71* (4), 1–7.

(45) Robson, R. E.; White, R. D.; Ness, K. F. *J. Chem. Phys.* **2011**, *134* (6), 064319.

(46) Seng, G.; Lindler, F. *J. Phys. B. Atom. Molec. Phys.* **1976**, *9* (14).

(47) Vermeiren, V.; Bogaerts, A. *J. Phys. Chem. C* **2019**, *123* (29), 17650–17665.

(48) Pietanza, L. D.; Colonna, G.; Ammando, G. D.; Laricchiuta, A.; Capitelli, M. *Phys. Plasmas* **2016**, *23* (013515).

(49) Silva, T.; Grofulović, M.; Klarenaar, B. L. M.; Morillo-Candas, A. S.; Guaitella, O.; Engeln, R.; Pintassilgo, C. D.; Guerra, V. *Plasma Sources Sci. Technol.* **2018**, *27* (1), 015019.

(50) Braunstein, M.; Conforti, P. F. *J. Phys. Chem. A* **2015**, No. 119, 3311–3322.

(51) Blauer, J. A. *A Survey of Vibrational Relaxation Rate Data Processes Important to CO2-N2-H2O Infrared Plume Radiation*; NTIS, 1973.

(52) Schwartz, R. N.; Slawsky, Z. I.; Herzfeld, K. F. *J. Chem. Phys.* **1952**, *20* (10), 1591–1599.

(53) Adamovich, I. V; Macheret, S.; Rich, J. W.; Treanor, C. E. *J. Thermophys. Heat Transf.* **1998**, *12* (1).

(54) Silva, T.; Grofulovic, M.; Terraz, L.; Pintassilgo, C. D.; Guerra, V. *J. Phys. D. Appl. Phys.* **2018**, *51*.

(55) Gamache, R. R.; Lynch, R.; Plateaux, J. J.; Barbe, A. *J. Quant. Spectrosc. Radiat. Transf.* **1997**, *57* (4), 485–496.

(56) Ramakers, M.; Trenchev, G.; Heijkers, S.; Wang, W.; Bogaerts, A. *ChemSusChem* **2017**, *10*, 2642–2652.

(57) Slaets, J.; Aghaei, M.; Ceulemans, S.; Van Alphen, S.; Bogaerts, A. *Green Chem.* **2020**, *22*, 1366–1377.

(58) Sun, S. R.; Wang, H. X.; Mei, D. H.; Tu, X.; Bogaerts, A. *J. CO2 Util.* **2017**, *17*, 220–234.

(59) Aerts, R.; Somers, W.; Bogaerts, A. *ChemSusChem* **2015**, *8* (4), 702–716.

(60) Snoeckx, R.; Zeng, Y. X.; Tu, X.; Bogaerts, A. *RSC Adv.* **2015**, *5* (38), 29799–29808.

(61) Wang, W.; Snoeckx, R.; Zhang, X.; Cha, M. S.; Bogaerts, A. *J. Phys. Chem. C* **2018**, *122*, 8704–8723.

(62) NIST Chemical Webbook https://webbook.nist.gov/chemistry/.

(63) UNAM Database www.lxcat.net/UNAM.

(64) KIDA database http://kida.astrophy.u-bordeaux.fr/.

Appendix

A1. Vibrational-translational (VT) reactions between CO_2 vibrational levels and H_2O ground-state molecules, adopted from Blauer.[51]

The VT reactions between CO_2 vibrational levels and H_2O ground-state molecules are listed in Tables A1 and A2. Table A1 presents the rate coefficients calculated at 1500 K, while Table A2 lists the coefficients (A, B, C) needed to calculate the rate coefficients at any other temperature, using equation (10) in the paper.

Table A1: *Reactions and corresponding rate coefficients (at 1500 K) for the VT CO_2-H_2O reactions of the lower vibrational levels (including symmetric and asymmetric modes), adopted from Blauer.[51] For the higher asymmetric mode levels, we use the SSH scaling, as explained in the text. No scaling is needed for the higher symmetric mode levels, as they are not included in our model.*

Reaction	**k ($cm^3s^{-1}mol^{-1}$) (1500 K)**
$CO_2(01^10) + H_2O \rightarrow CO_2(00^00) + H_2O$	**$3.8x10^{12}$**
$CO_2(02^00, 10^00) + H_2O \rightarrow CO_2(01^10) + H_2O$	**$5.0x10^{11}$**
$CO_2(02^00, 10^00) + H_2O \rightarrow CO_2(00^00) + H_2O$	**$6.2x10^{10}$**
$CO_2(03^10, 11^10) + H_2O \rightarrow CO_2(02^00, 10^00) + H_2O$	**$1.5x10^{13}$**
$CO_2(03^10, 11^10) + H_2O \rightarrow CO_2(01^10) + H_2O$	**$3.5x10^{11}$**
$CO_2(00^01) + H_2O \rightarrow CO_2(02^00, 10^00) + H_2O$	**$1.3x10^{12}$**
$CO_2(00^01) + H_2O \rightarrow CO_2(03^10, 11^10) + H_2O$	**$1.5x10^{11}$**
$CO_2(00^01) + H_2O \rightarrow CO_2(01^10) + H_2O$	**$1.3x10^{11}$**
$CO_2(04^00, 12^00, 20^00) + H_2O \rightarrow CO_2(00^01) + H_2O$	**$8.7x10^{9}$**
$CO_2(04^00, 12^00, 20^00) + H_2O \rightarrow CO_2(03^10, 11^10) + H_2O$	**$2.3x10^{13}$**
$CO_2(04^00, 12^00, 20^00) + H_2O \rightarrow CO_2(02^00, 10^00) + H_2O$	**$3.7x10^{11}$**

Table A2: *Constants used to calculate the rate coefficients for the VT CO_2-H_2O reactions of the lower vibrational levels (including symmetric and asymmetric modes), at any temperature in the range of 300 - 3000 K (see equation (10) in the paper, adopted from Blauer.[51]*

Reaction	A	B	C
$CO_2(01^10) + H_2O \rightarrow CO_2(00^00) + H_2O$	31.0	-44.4	242
$CO_2(02^00, 10^00) + H_2O \rightarrow CO_2(01^10) + H_2O$	29.0	-44.4	242
$CO_2(02^00, 10^00) + H_2O \rightarrow CO_2(00^00) + H_2O$	26.8	-44.0	242
$CO_2(03^10, 11^10) + H_2O \rightarrow CO_2(02^00, 10^00) + H_2O$	32.4	-44.4	242

$CO_2(03^10, 11^10) + H_2O \rightarrow CO_2(01^10) + H_2O$	43.0	-234	525
$CO_2(00^01) + H_2O \rightarrow CO_2(02^00, 10^00) + H_2O$	27.9	18.5	-211
$CO_2(00^01) + H_2O \rightarrow CO_2(03^10, 11^10) + H_2O$	19.3	108	-397
$CO_2(00^01) + H_2O \rightarrow CO_2(01^10) + H_2O$	30.7	-54.7	-36
$CO_2(04^00, 12^00, 20^00) + H_2O \rightarrow CO_2(00^01) + H_2O$	29.1	-85.3	159
$CO_2(04^00, 12^00, 20^00) + H_2O \rightarrow CO_2(03^10, 11^10) + H_2O$	32.8	-44.4	242
$CO_2(0400, 12^00, 20^00) + H_2O \rightarrow CO_2(02^00, 10^00) + H_2O$	42.2	-215	430

For the asymmetric mode levels, the following general reaction is used, for which the rate coefficients can be calculated for the higher levels at any gas temperature:

Reaction	**k (cm^3s^{-1})**
$CO_2(00^0v) + H_2O \rightarrow CO_2(00^0(v-1)) + H_2O$	$\exp((28.08)+(8.97) \times Tgas^{(-1/3)}+(-109.57) \times Tgas^{(-2/3)})x1.66113x10^{-24}$

A2. CO_2 Cross Section set as adapted from Vermeiren et al.[47]

Table A3: *Cross Section set adapted from Vermeiren et al.*[47]

Reaction
$e + CO_2 \rightarrow 2e + CO_2^+$
$e + CO_2 \rightarrow 2e + O + CO^+$
$e + CO_2 \rightarrow O^- + CO$
$e + CO_2 \rightarrow e + O + CO$
$e + CO_2 \rightarrow e + CO_2[e_1]$
$e + CO_2 \leftrightarrow e + CO[v_i]$ i=a,b,c,d
$e + CO_2[v_i] \leftrightarrow e + CO_2[v_j]$ i,j=0-21
$e + CO \rightarrow 2e + CO^+$
$e + CO \rightarrow C + O^-$
$e + CO \rightarrow e + C + O$
$e + CO \rightarrow e + CO[e_x]$ x=1-4
$e + CO \rightarrow e + CO[v_i]$ i=1-10
$e + O_2 \rightarrow e + O + O$
$e + O_2 + M \rightarrow e + O^- 2 + M$
$e + O_2 \rightarrow O + O^s$
$e + O_2 \leftrightarrow e + O2[v_i]$ i=1,2,3
$e + O_2 \leftrightarrow e + O2[e_x]$

Note that the CO_2 vibrational, electronic and dissociative attachment cross sections are adapted from Grofulovic et al.[20] The other CO_2 cross sections are adapted from the Phelps LxCat database.[31] Therefore, we have tested the swarm parameters with values from the UNAM LxCat database.[63]

For the vibrationally and electronically excited species, the superelastic collisions are added, indicated by the double arrow in Table A3. The significance of the superelastic collisions is demonstrated in Figure A2.2 for different reduced electric fields.

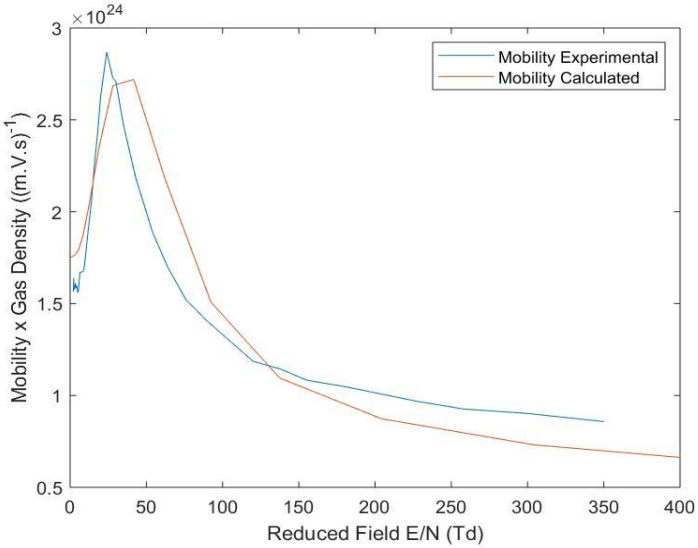

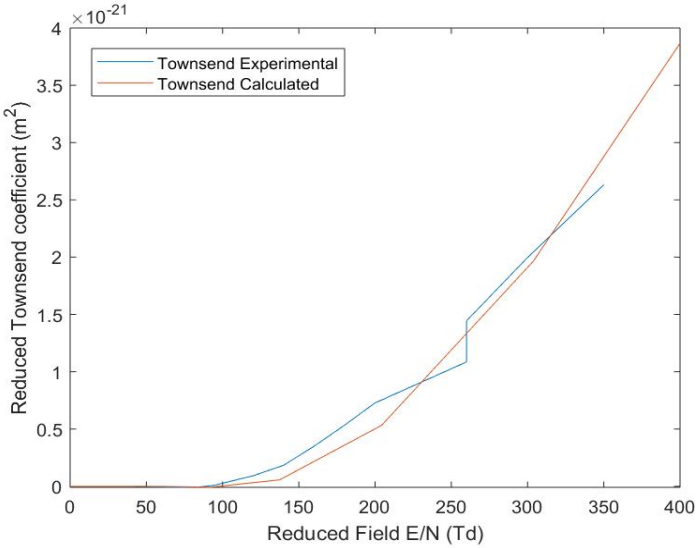

Figure A2.1 Swarm parameter test for the CO_2 cross section set adapted from Vermeiren et al.[47].

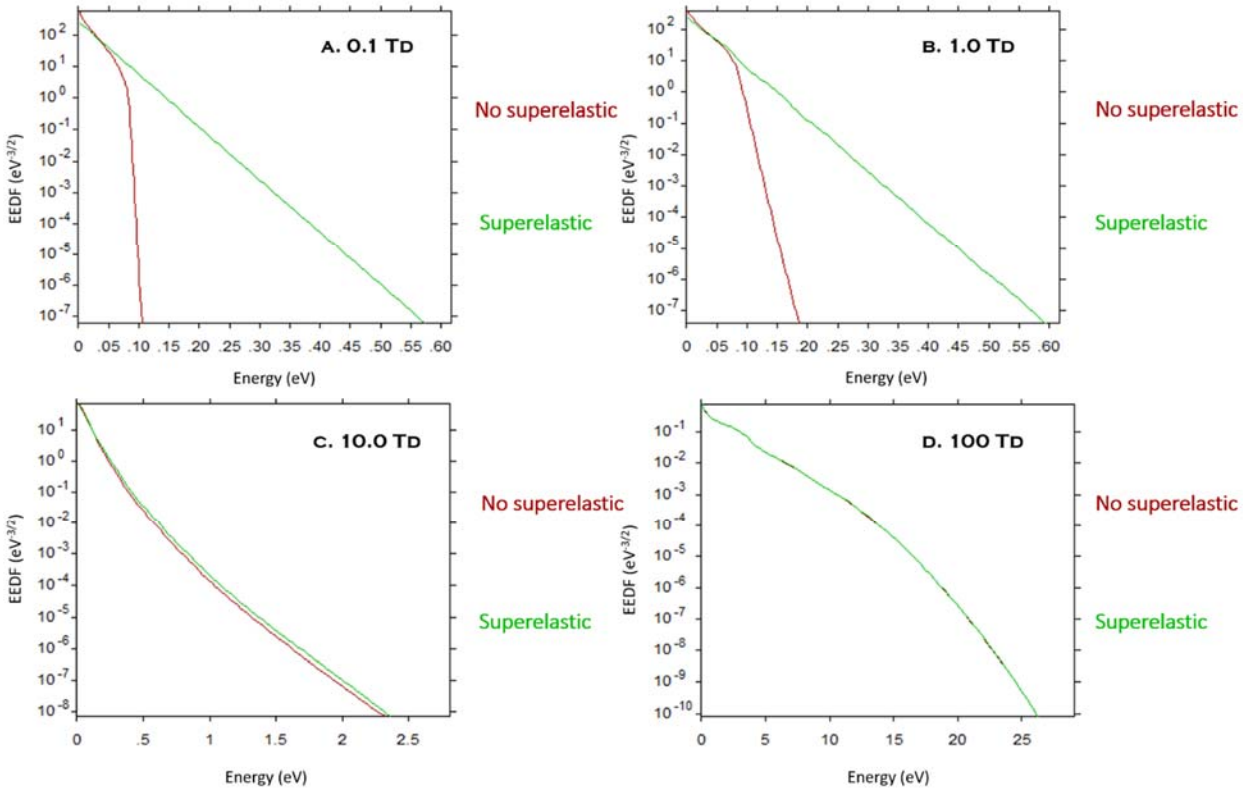

Figure A2.2 EEDF for different reduced electric fields calculated by Bolsig+.[21] *As can be seen in A and B, for lower electric fields, the superelastic collisions will cause significant difference, while for higher fields as in C and D, superelastic collisions play a less important role.*

A3. Reactions for the Chemistry in the CO_2/H_2O plasma

Table A4: *Reactions from Vermeiren et al.*[47]

Reaction	**k (cm^3s^{-1})**
$CO_2v_a + M \rightarrow CO_2 + M$	$7.14 \times 10^{-15} \exp(-177\ T_{gas}^{-1/3} + 451 T_{gas}^{-2/3})$
$CO_2v_1 + M \rightarrow CO_2v_a + M$	$4.25 \times 10^{-7} \exp(-407\ T_{gas}^{-1/3} + 824 T_{gas}^{-2/3})$
$CO_2v_1 + M \rightarrow CO_2v_b + M$	$8.57 \times 10^{-7} \exp(-404\ T_{gas}^{-1/3} + 1096 T_{gas}^{-2/3})$
$CO_2v_1 + M \rightarrow CO_2v_c + M$	$1.43 \times 10^{-7} \exp(-252\ T_{gas}^{-1/3} + 685 T_{gas}^{-2/3})$
$COv_1 + M \rightarrow CO + M$	$1.0 \times 10^{-18}\ T_{gas} \exp(-150.7\ T_{gas}^{-1/3})$
$O_2v_1 + M \rightarrow O_2 + M$	$1.3 \times 10^{-14}\ T_{gas} \exp(-158.7\ T_{gas}^{-1/3})$
$CO_2v_1 + CO2 \rightarrow CO_2v_a + CO_2v_b$	$1.06 \times 10^{-11} \exp(-242\ T_{gas}^{-1/3} + 633 T_{gas}^{-2/3})$
$CO_2v_1 + CO2 \rightarrow CO_2 + CO_2v_1$	$1.32 \times 10^{-16}\ (T_{gas}/300)^{0.5}(\ 200/\ T_{gas})$
$COv_1 + CO \rightarrow CO + COv_1$	$3.4 \times 10^{-16}\ (T_{gas}/300)^{0.5}(1.64 \times 10^{-6} T_{gas}(1.61/\ T_{gas}))$
$CO_2v_1 + CO \rightarrow CO_2 + COv_1$	$4.8 \times 10^{-12} \exp(-153 T_{gas}^{-1/3})$

$CO_2 + M \rightarrow CO + O + M$	$6.06 \times 10^{-16} \exp(-52525/T_{gas})$
$CO_2 + O \rightarrow CO + O_2$	$2.8 \times 10^{-17} \exp(-16400/T_{gas})$
$CO_2 + C \rightarrow 2CO$	$< 10^{-21}$
$CO + O + M \rightarrow CO_2 + M$	$8.3 \times 10^{-46} \exp(-1510/T_{gas})$**
$O_2 + CO \rightarrow CO_2 + O$	$4.2 \times 10^{-18} \exp(-24000/T_{gas})$
$O_2 + C \rightarrow CO + O$	$1.99 \times 10^{-16} \exp(-2010/T_{gas})$
$O + C + M \rightarrow CO + M$	$2.14 \times 10^{-41} (T_{gas}/300)^{-3.08} \exp(-2144/ T_{gas})$
$O + O + M \rightarrow O_2 + M$	$5.2 \times 10^{-47} \exp(900/T_{gas})$
$O_2 + M \rightarrow O + O + M$	$3.0 \times 10^{-12} (1/ T_{gas}) \exp(-59380/T_{gas})$
$CO_2 + CO^+ \rightarrow CO_2^+ + CO$	1.0×10^{-15}
$CO_2 + O^- + CO_2 \rightarrow CO_3^- + CO_2$	1.5×10^{-40}
$CO_2 + O^- + CO \rightarrow CO_3^- + CO$	1.5×10^{-40}
$CO_2 + O^- + O_2 \rightarrow CO_3^- + O_2$	3.1×10^{-40}
$CO_2 + O^-_2 + M \rightarrow CO_4^- + M$	4.7×10^{-41}
$CO + O^- \rightarrow CO_2 + e$	5.5×10^{-16}
$CO + CO_3^- \rightarrow 2CO_2 + e$	5×10^{-19}
$CO_3^- + CO_2^+ \rightarrow 2CO_2v_b + O$	5×10^{-13}
$CO_4^- + CO_2^+ \rightarrow 2CO_2v_b + O2$	5×10^{-13}
$O_2^- + CO_2^+ \rightarrow CO_2v_1 + O_2 + O$	6×10^{-13}
$CO_3^- + O \rightarrow CO_2 + O^-$	8×10^{-17}
$CO_4^- + O \rightarrow CO_3^- + O_2$	1.12×10^{-16}
$CO_4^- + O \rightarrow CO_2 + O_2 + O^-$	1.4×10^{-17}
$O + O^- \rightarrow O_2 + e$	2.3×10^{-16}
$O + O_2^- \rightarrow O_2 + O^-$	1.5×10^{-16}
$O_2^- + M \rightarrow O_2 + M + e$	$2.7 \times 10^{-16} (T_{gas}/300)^{0.5} \exp(-5590/ T_{gas})$
$O^- + M \rightarrow O + M + e$	$2.3 \times 10^{-15} \exp(-26000/ T_{gas})$
$e + CO_2^+ \rightarrow COv_1 + O$	$1.0 \times 10^{-11} T_e^{-0.5} T_{gas}^{-1}$
$e + CO_2^+ \rightarrow C + O_2$	$1.0 \times 10^{-11} T_e^{-0.5} T_{gas}^{-1}$
$e + CO_4^+ \rightarrow CO_2 + O_2$	$1.61 \times 10^{-13} T_e^{-0.5}$
$e + CO^+ \rightarrow C + O$	$3.46 \times 10^{-14} T_e^{-0.48}$
$e + O + M \rightarrow O^- + M$	1×10^{-43}

** Multiply by 7, 3 or 12 for M= CO_2, CO or O_2 respectively.

Table A5: *Neutral-Neutral Reactions from NIST database.*[62]

Reaction	**k (cm^3s^{-1})**
$H_2O + CH_2 \rightarrow CH_3 + OH$	1.6×10^{-16}
$H_2O + O \rightarrow OH + OH$	$1.84 \times 10^{-11} \times (T_{gas}/298)^{0.95} \times \exp((-71.26 \times 10^3)/(RTgas))$
$H_2O + O \rightarrow HO_2 + H$	$4.48 \times 10^{-12} \times (T_{gas}/298)^{0.97} \times \exp((-287 \times 10^3)/(RTgas))$
$H_2O + O \rightarrow H_2 + O_2$	$4.48 \times 10^{-12} \times (T_{gas}/298)^{0.97} \times \exp((-287 \times 10^3)/(RTgas))$
$H_2O + H \rightarrow H_2 + OH$	$1.58 \times 10^{-11} \times (T_{gas}/298)^{1.20} \times \exp((-79.90 \times 10^3)/(RTgas))$
$H_2O + O_3 \rightarrow H_2O2 + O_2$	1.1×10^{-22}
$H_2O + O_2 \rightarrow HO_2 + OH$	$7.72 \times 10^{-12} \times \exp((-310 \times 10^3)/(RTgas))$
$H_2O + H_2O \rightarrow OH + H_2O + H$	$1.8 \times 10^{-8} \times e(-446 \times 10^3)/(RTgas)$
$H_2O + H + OH \rightarrow H_2O + H_2O$	$1.19 \times 10^{-30} \times (T_{gas}/298)^{-2.10}$
$H_2O + C \rightarrow CH + OH$	$1.3 \times 10^{-12} \times \exp((-165 \times 10^3)/(RTgas))$
$H_2O + OH + H \rightarrow H_2O + H_2O$	$1.19 \times 10^{-30} \times (T_{gas}/298)^{-2.10}$
$H_2O + CH \rightarrow CH_2OH$	$9.48 \times 10^{-12} \times \exp((3.16 \times 10^3)/(RTgas))$
$H_2O + CH \rightarrow CH_2O + H$	$2.82 \times 10^{-11} \times (T_{gas}/298)^{-1.22} \times \exp((0.10 \times 10^3)/(RTgas))$
$H_2O + HO_2 \rightarrow OH + H_2O_2$	$4.65 \times 10^{-11} \times \exp((-137 \times 10^3)/(RTgas))$
$H_2O + HCO \rightarrow CH_2O + OH$	$8.54 \times 10^{-13} \times (T_{gas}/298)^{1.35} \times \exp((-109 \times 10^3)/(RTgas)$
$H_2O + CH_2OH \rightarrow CH_3OH + OH$	$4.12 \times 10^{-14} \times (T_{gas}/298)^{3.00} \times \exp((-86.80 \times 10^3)/(RTgas))$
$H_2O + CH_3O \rightarrow CH_3OH + OH$	$1.46 \times 10^{-15} \times (T_{gas}/298)^{3.80} \times \exp((-48.06 \times 10^3)/(RTgas))$
$H_2O + CH_2O \rightarrow CH_3 + HO_2$	$4.09 \times 10^{-15} \times (T_{gas}/298)^{2.68} \times \exp((-429 \times 10^3)/(RTgas))$
$CH_3OH + H \rightarrow CH_3 + H_2O$	$3.32 \times 10^{-10} \times \exp((-22.20 \times 10^3)/(RT_{gas}))$
$CH_3OH + OH \rightarrow CH_2OH + H_2O$	$2.13 \times 10^{-13} \times (T_{gas}/298)^{-2.00} \times \exp((3.52 \times 10^3)/(RT_{gas}))$
$CH_3OH + OH \rightarrow CH_2O + H + H_2O$	$1.1 \times 10^{-12} \times (T_{gas}/298)^{1.44} \times \exp((-0.47 \times 10^3)/(RTgas))$
$CH_3OH + OH \rightarrow CH_3O + H_2O$	$1.66 \times 10^{-11} \times \exp((3.52 \times 10^3)/(RT_{gas}))$
$CH_2O + OH \rightarrow HCO + H_2O$	$4.73 \times 10^{-12} \times (Tgas/298)^{**(1.18)*} \times \exp((1871)/(R \times Tgas))$
$O_2 + CH_2 \rightarrow CO + H_2O$	$2.54 \times 10^{-10} \times (T_{gas}/298)^{-3.30} \times \exp((-11.97 \times 10^3)/(RT_{gas}))$
$H_2O_2 + H \rightarrow OH + H_2O$	$4.00 \times 10^{-11} \times \exp((-16.63 \times 10^3)/(RT_{gas}))$
$H_2O_2 + O_3 \rightarrow O_2 + O_2 + H_2O$	4.00×10^{-20}
$OH + H_2O_2 \rightarrow HO_2 + H_2O$	$2.90 \times 10^{-12} \times \exp((-1.33 \times 10^3)/(RT_{gas}))$
$OH + OH \rightarrow H_2O + O$	$5.15 \times 10^{-14} \times (T_{gas}/298)^{2.40} \times \exp((8.81 \times 10^3)/(RTgas))$
$HO_2 + H \rightarrow H_2O + O$	2.40×10^{-12}
$HO_2 + OH \rightarrow H_2O + O_2$	$4.80 \times 10^{-11} \times \exp((2.08 \times 10^3)/(RT_{gas}))$
$H_2 + O_2 \rightarrow H_2O + O$	$4.15 \times 10^{-11} \times (T_{gas}/298)^{0.51} \times \exp((-295 \times 10^3)/(RT_{gas}))$
$HCO + OH \rightarrow CO + H_2O$	1.69×10^{-10}

$CH_2OH + OH \rightarrow CH_2O + H_2O$	4.00×10^{-11}
$CH_3 + OH \rightarrow H_2O + CH_2$	$1.20 \times 10^{-10} \times \exp((-11.64 \times 10^3)/(RT_{gas}))$
$CH_3O + OH \rightarrow CH_2O + H_2O$	3.01×10^{-11}
$H_2 + OH \rightarrow H_2O + H$	$2.06 \times 10^{-12} \times (T_{gas}/298)^{1.52} \times \exp((-14.47 \times 10^3)/(RT_{gas}))$
$CO_2 + CH_2 \rightarrow CH_2O + CO$	3.9×10^{-14}
$CO_2 + H \rightarrow CO + OH$	$2.51 \times 10^{-10} \times \exp((-111 \times 10^3)/(RT_{gas}))$
$O_2 + CH_2 \rightarrow CO_2 + H_2$	$2.99 \times 10^{-11} \times (T_{gas}/298)^{-3.30} \times \exp((-11.97 \times 10^3)/(RT_{gas}))$
$O_2 + CH_2 \rightarrow CO_2 + H + H$	$3.74 \times 10^{-11} \times (T_{gas}/298)^{-3.30} \times \exp((-11.97 \times 10^3)/(RT_{gas}))$
$HCO + O \rightarrow CO_2 + H$	5.0×10^{-11}
$HCO + O_3 \rightarrow CO_2 + O_2 + H$	8.3×10^{-13}
$CO + O_3 \rightarrow CO_2 + O_2$	4.0×10^{-25}
$CO + OH \rightarrow CO_2 + H$	$5.4 \times 10^{-14} \times (T_{gas}/298)^{1.50} \times \exp((2.08 \times 10^3)/(RT_{gas}))$
$CH_3O + CO \rightarrow CO_2 + CH_3$	$2.61 \times 10^{-11} \times \exp((-49.39 \times 10^3)/(RT_{gas}))$
$HO_2 + CO \rightarrow CO_2 + OH$	$2.51 \times 10^{-10} \times \exp((-98.94 \times 10^3)/(RT_{gas}))$
$CO + H\cdot \rightarrow HCO$	$5.29 \times 10^{-34} \times \exp((-3.08 \times 10^3)/(RT_{gas}))$
$O\cdot + \cdot CH_2 \rightarrow CO + H\cdot + H\cdot$	1.33×10^{-10}
$O\cdot + \cdot CH_2 \rightarrow CO + H_2$	6.64×10^{-11}
$\cdot CH + O\cdot \rightarrow CO + H\cdot$	6.59×10^{-11}
$\cdot CH + O_2 \rightarrow CO + \cdot OH$	8.3×10^{-11}
$HCO + \cdot CH_2 \rightarrow CO + \cdot CH_3$	3.01×10^{-11}
$HCO + O_2 \rightarrow CO + HO_2$	$8.5 \times 10^{-11} \times \exp((-7.07 \times 10^3)/(RT_{gas}))$
$HCO + M \rightarrow CO + H\cdot + M$	$4.3 \times 10^{-8} \times (T_{gas}/298)^{-2.14} \times \exp((-85.64 \times 10^3)/(RT_{gas}))$
$CH_3 + HCO \rightarrow CH_4 + CO$	2.01×10^{-10}
$CH_3O\cdot + HCO \rightarrow CH_3OH + CO$	1.5×10^{-10}
$CH_2O \rightarrow CO + H_2$	$3.49 \times 10^{-9} \times \exp((-146 \times 10^3)/(RT_{gas}))$
$HCO + H\cdot \rightarrow CO + H_2$	1.5×10^{-10}
$H_2 + \cdot CH_2 \rightarrow \cdot CH_3 + H\cdot$	5.0×10^{-15}
$H_2 + O\cdot \rightarrow \cdot OH + H\cdot$	$3.44 \times 10^{-13} \times (T_{gas}/298)^{2.67} \times \exp((-26.27 \times 10^3)/(RT_{gas}))$
$H_2 + O_2 \rightarrow \cdot OH + \cdot OH$	$4.17 \times 10^{-12} \times \exp((-163 \times 10^3)/(RT_{gas}))$
$H_2 + O_2 \rightarrow HO_2 + H\cdot$	$2.41 \times 10^{-10} \times \exp((-237 \times 10^3)/(RT_{gas}))$
$H_2 + \cdot CH \rightarrow H\cdot + \cdot CH_2$	$1.48 \times 10^{-11} \times (T_{gas}/298)^{1.79} \times \exp((-6.98 \times 10^3)/(RT_{gas}))$
$H_2 + \cdot CH \rightarrow \cdot CH_3$	$2.01 \times 10^{-10} \times (T_{gas}/298)^{0.15}$

$H_2 + HO_2 \rightarrow H_2O_2 + H\cdot$	$5.0 \times 10^{-11} \times \exp((-3.08\times10^3)/(RT_{gas})) \times \exp((-109\times10^3)/(RT_{gas}))$
$H_2 + HCO \rightarrow CH_2O + H\cdot$	$2.66 \times 10^{-13} \times (T_{gas}/298)^{2.00} \times \exp((-74.58\times10^3)/(RT_{gas}))$
$H_2 + CH_3O\cdot \rightarrow CH_3OH + H\cdot$	$1.66 \times 10^{-15} \times (T_{gas}/298)^{4.00} \times \exp((-20.54\times10^3)/(RT_{gas}))$
$H_2 + M \rightarrow H\cdot + H\cdot + M$	$3.7 \times 10^{-10} \times \exp((-402\times10^3)/(RT_{gas}))$
$CH_2O + H_2 \rightarrow CH_3OH$	$2.29 \times 10^{-11} \times \exp((-292\times10^3)/(RT_{gas}))$
$\cdot CH_2 + M \rightarrow H_2 + C + M$	$2.66 \times 10^{-10} \times \exp((-268\times10^3)/(RT_{gas}))$
$H\cdot + \cdot CH_2 \rightarrow H_2 + \cdot CH$	$1.0 \times 10^{-11} \times \exp((7.48\times10^3)/(RT_{gas}))$
$H\cdot + H\cdot + M \rightarrow H_2 + M$	$6.04 \times 10^{-33} \times (T_{gas}/298)^{-1.00}$
$OH + H\cdot \rightarrow H_2 + O\cdot$	$6.86 \times 10^{-14} \times (T_{gas}/298)^{2.80} \times \exp((-16.21\times10^3)/(RT_{gas}))$
$\cdot OH + \cdot OH \rightarrow H_2 + O_2$	$3.32 \times 10^{-12} \times (T_{gas}/298)^{0.51} \times \exp((-211\times10^3)/(RT_{gas}))$
$HO_2 + H\cdot \rightarrow H_2 + O_2$	$1.1 \times 10^{-10} \times \exp((-3.08\times10^3)/(RT_{gas})) \times \exp((-8.90\times10^3)/(RT_{gas}$
$\cdot CH_3 + \cdot OH \rightarrow CH_2O + H_2$	$2.59 \times 10^{-13} \times (T_{gas}/298)^{-0.53} \times \exp((-45.23\times10^3)/(RT_{gas}))$
$CH_3OH + H\cdot \rightarrow H_2 + CH_3O\cdot$	$6.64 \times 10^{-11} \times \exp((-3.08\times10^3)/(RT_{gas})) \times \exp((-25.53\times10^3)/(RT_{gas}))$
$CH_3OH + H\cdot \rightarrow H_2 + CH_2OH$	$2.42 \times 10^{-12} \times (T_{gas}/298)^{2.00} \times \exp((-18.87\times10^3)/(RT_{gas}))$
$\cdot CH_3 + \cdot OH \rightarrow CH_3OH$	$2.25 \times 10^{-24} \times (T_{gas}/298)^{-8.20}$
$\cdot CH_3 + \cdot OH \rightarrow CH_3O\cdot + H\cdot$	$2.57 \times 10^{-12} \times (T_{gas}/298)^{-0.23} \times \exp((-58.28\times10^3)/(RT_{gas}))$
$\cdot CH_3 + \cdot OH \rightarrow CH_2OH + H\cdot$	$1.54 \times 10^{-9} \times (T_{gas}/298)^{-1.80} \times \exp((-33.76\times10^3)/(RT_{gas}))$
$\cdot OH + M \rightarrow H\cdot + O\cdot + M$	$4.0 \times 10^{-9} \times \exp((-416\times10^3)/(RT_{gas}))$
$\cdot OH + \cdot OH \rightarrow HO_2 + H\cdot$	$3.32 \times 10^{-12} \times (T_{gas}/298)^{0.51} \times \exp((-211\times10^3)/(RT_{gas}))$
$\cdot OH + \cdot OH \rightarrow H_2O_2$	$6.04 \times 10^{-31} \times (T_{gas}/298)^{-3.00}$
$OH + H_2O_2 \rightarrow HO_2 + H_2O$	$2.91 \times 10^{-12} \times \exp((-1.33\times10^3)/(RT_{gas}))$
$\cdot OH + O\cdot \rightarrow O_2 + H\cdot$	$4.33 \times 10^{-11} \times (T_{gas}/298)^{-0.50} \times \exp((-0.25\times10^3)/(RT_{gas}))$
$\cdot OH + \cdot CH_2 \rightarrow CH_2O + H\cdot$	3.01×10^{-11}
$O_2 + H\cdot \rightarrow \cdot OH + O\cdot$	$1.22 \times 10^{-11} \times (T_{gas}/298)^{0.96} \times \exp((-51.20\times10^3)/(RT_{gas}))$
$O_3 + H\cdot \rightarrow \cdot OH + O_2$	$1.4 \times 10^{-10} \times \exp((-3.91\times10^3)/(RT_{gas}))$
$H\cdot + O\cdot + M \rightarrow \cdot OH + M$	$4.36 \times 10^{-32} \times (T_{gas}/298)^{-1.00}$
$CH_2O + O\cdot \rightarrow HCO + \cdot OH$	$1.78 \times 10^{-11} \times (T_{gas}/298)^{0.57} \times \exp((-11.56\times10^3)/(RT_{gas}))$
$CH_3OH \rightarrow \cdot CH_3 + \cdot OH$	$1.9 \times 10^{16} \times \exp((-384\times10^3)/(RT_{gas}))$
$CH_3OH + O\cdot \rightarrow \cdot CH_2OH + \cdot OH$	$1.63 \times 10^{-11} \times \exp((-18.87\times10^3)/(RT_{gas}))$
$CH_3O\cdot + O\cdot \rightarrow CH_2O + \cdot OH$	1.0×10^{-11}
$\cdot CH_3 + HO_2 \rightarrow CH_3O\cdot + \cdot OH$	3.01×10^{-11}

$\cdot CH_3 + O_2 \rightarrow CH_2O + \cdot OH$	$3.11 \times 10^{-13} \times \exp((-41.18 \times 10^3)/(RT_{gas}))$
$\cdot CH_2OH + O\cdot \rightarrow CH_2O + \cdot OH$	7.01×10^{-11}
$HCO + O\cdot \rightarrow CO + \cdot OH$	5.0×10^{-11}
$HO_2 + O_3 \rightarrow \cdot OH + O_2 + O_2$	$1.97 \times 10^{-16} \times (T_{gas}/298)^{4.57} \times \exp((5.76 \times 10^3)/(RT_{gas}))$
$HO_2 + O\cdot \rightarrow \cdot OH + O_2$	$2.7 \times 10^{-11} \times \exp((1.86 \times 10^3)/(RT_{gas}))$
$CH + O\cdot \rightarrow \cdot OH + C$	$2.52 \times 10^{-11} \times \exp((-19.79 \times 10^3)/(RT_{gas}))$
$H_2O_2 \rightarrow \cdot OH + \cdot OH$	$2.01 \times 10^{-7} \times \exp((-190 \times 10^3)/(RT_{gas}))$
$CH_2OH + H\cdot \rightarrow \cdot CH_3 + \cdot OH$	1.6×10^{-10}
$CH_3O\cdot + HO_2 \rightarrow CH_2O + H_2O_2$	5.0×10^{-13}
$CH_2OH + HO_2 \rightarrow CH_2O + H_2O_2$	2.01×10^{-11}
$HO_2 + O_3 \rightarrow HO_3 + O_2$	$1.23 \times 10^{-16} \times (T_{gas}/298)^{5.37} \times \exp((7.36 \times 10^3)/(RT_{gas}))$
$HO_2 + M \rightarrow O_2 + H\cdot + M$	$2.41 \times 10^{-8} \times (T_{gas}/298)^{-1.18} \times \exp((-203 \times 10^3)/(RT_{gas}))$
$CH_3OH + HO_2 \rightarrow \cdot CH_2OH + H_2O_2$	$1.6 \times 10^{-13} \times \exp((-52.63 \times 10^3)/(RT_{gas}))$
$O_3 + H\cdot \rightarrow HO_2 + O\cdot$	7.51×10^{-13}
$O_2 + H\cdot + M \rightarrow HO_2 + M$	$6.09 \times 10^{-32} \times (T_{gas}/298)^{-0.80}$
$H_2O_2 + O_2 \rightarrow HO_2 + HO_2$	$9.0 \times 10^{-11} \times \exp((-166 \times 10^3)/(RT_{gas}))$
$H_2O_2 + H\cdot \rightarrow H_2 + HO_2$	$2.81 \times 10^{-12} \times \exp((-15.71 \times 10^3)/(RT_{gas}))$
$M + O_2 + H\cdot \rightarrow M + HO_2$	$5.47 \times 10^{-32} \times (T_{gas}/298)^{-1.8}$
$O_3 + M \rightarrow O_2 + O\cdot + M$	$7.16 \times 10^{-10} \times \exp((-93.12 \times 10^3)/(RT_{gas}))$
$O_3 + O\cdot \rightarrow O_2 + O_2$	$8.0 \times 10^{-12} \times \exp((-17.13 \times 10^3)/(RT_{gas}))$
$M + O_2 + O\cdot \rightarrow M + O_3$	$5.7 \times 10^{-34} \times (T_{gas}/298)^{-2.60}$
$O_2 + O_2 \rightarrow O_3 + O\cdot$	1.11×10^{-11}

Table A6: *Ion-Neutral and Ion-Ion Reactions from KIDA database*[64]

Reaction	**k ($cm^3s^{-1}mol^{-1}$)**
$H + O^+ \rightarrow O + H^+$	7.00×10^{-10}
$H^+ + OH^- \rightarrow H + OH$	$7.51 \times 10^{-8} \times (T_e/300)^{-0.5}$
$H^+ + O \rightarrow H + O^+$	$7.00 \times 10^{-10} \times \exp(-2.32 \times 10^2/T_{gas})$
$H + O^- \rightarrow OH + e^-$	5.00×10^{-10}
$CO^+ + H \rightarrow CO + H^+$	3.40×10^{-10}
$CO_2^+ + H \rightarrow CO_2 + H^+$	1.00×10^{-10}
$H + H^- \rightarrow H_2 + e^-$	1.30×10^{-9}

$CO_2^+ + O \rightarrow CO + O_2^+$	$1.64x10^{-10}$
$CO_2^+ + O_2 \rightarrow CO_2 + O_2^+$	$5.00x10^{-11}$
$CO_2^+ + O \rightarrow CO_2 + O^+$	$9.62x10^{-11}$
$CO_2^+ + H_2O \rightarrow CO_2 + H_2O^+$	$0.73 \times 7.76x10^{-10} \times (0.62 + 0.4767 \times 5.41 \times (300/T_{gas})^{0.5})$
$CO_2^+ + e^- \rightarrow O + CO$	$4.20x10^{-7} \times (T_e/300)^{-0.75}$
$CH + O^+ \rightarrow H + CO^+$	$0.5 \times 1.27x10^{-9} \times (0.62 + 0.4767 \times 3.33 \times (300/T_e)^{0.5})$
$C + O_2^+ \rightarrow O + CO^+$	5.20×10^{-11}
$CO^+ + O \rightarrow CO + O^+$	1.40×10^{-10}
$CO^+ + O_2 \rightarrow CO + O_2^+$	1.20×10^{-10}
$H_2O^+ + O \rightarrow H_2 + O_2^+$	4.00×10^{-11}
$O^+ + OH \rightarrow H + O_2^+$	$0.5 \times 8.45x10^{-10} \times (0.62 + 0.4767 \times 5.50 \times (300/T_e)^{0.5})$
$CO_2 + O^+ \rightarrow CO + O_2^+$	1.10×10^{-9}
$H_2 + O_2^+ \rightarrow H + H + O_2^+$	$3.00 \times 10^{-11} \times (T_{gas}/300)^{0.5} \times \exp(-5.20x10^4/T_{gas})$
$H_2O^+ + O_2 \rightarrow H_2O + O_2^+$	4.30×10^{-10}
$O^+ + O_2 \rightarrow O + O_2^+$	$1.3 \times 10^{-12} \times (T_{gas}/300)^{1.2}$
$H^+ + O_2 \rightarrow H + O_2$	1.20×10^{-9}
$O_2 + OH^+ \rightarrow OH + O_2^+$	5.90×10^{-10}
$H_2 + O^+ \rightarrow H + OH^+$	1.60×10^{-9}
$O_2^+ + e^- \rightarrow O + O$	$1.95 \times 10^{-7} \times (T_e/300)^{-0.7}$
$H_2 + O^- \rightarrow H + OH^-$	3.00×10^{-11}
$H^+ + O^- \rightarrow H + O$	$7.51 \times 10^{-8} \times (T_e/300)^{-0..5}$
$C + O^- \rightarrow CO + e^-$	5.00×10^{-10}
$H_2 + O^- \rightarrow H_2O + e^-$	7.00×10^{-10}
$H^- + O^+ \rightarrow H + O$	$2.30 \times 10^{-7} \times (T_e/300)^{-0..5}$
$H_2O + O^+ \rightarrow O + H_2O^+$	$9.54 \times 10^{-10} \times (0.62 + 0.4767 \times 5.41 \times (300/T_e)^{0.5})$
$O^+ + OH \rightarrow O + OH^+$	$0.5 \times 8.45 \times 10^{-10} \times (0.62 + 0.4767 \times 5.50 \times (300/T_e)^{0.5})$
$H^- + H_2O \rightarrow H_2 + OH^-$	4.80×10^{-9}
$H^+ + H^- \rightarrow H + H$	$2.30 \times 10^{-7} \times (T_e/300)^{-0.5}$
$C + H^- \rightarrow CH + e^-$	1.00×10^{-9}
$H^- + O \rightarrow OH + e^-$	1.00×10^{-9}
$CH + H^- \rightarrow CH_2 + e^-$	1.00×10^{-10}
$CO + H^- \rightarrow HCO + e^-$	2.00×10^{-11}
$H^- + OH \rightarrow H_2O + e^-$	1.00×10^{-10}
$H + e^- + M \rightarrow H^- + M$	3.00×10^{-16}

$CH_3 + OH^- \rightarrow CH_3OH + e^-$	1.00×10^{-9}
$H + H_3O^+ \rightarrow H_2 + H_2O^+$	$6.10 \times 10^{-10} \exp(-2.05 \times 10^4 / T_{gas})$
$H_2^+ + H_2O \rightarrow H + H_3O^+$	$4.66 \times 10^{-1} \times 2.07 \times 10^{-9} \times (0.62 + 0.4767 \times 5.41 \times (300/T_e)^{0.5})$
$H^- + H_3O^+ \rightarrow H + H_2 + OH$	$2.30 \times 10^{-7} \times (T_e/300)^{-0.5}$
$H^- + H_3O^+ \rightarrow H_2 + H_2O$	$2.30 \times 10^{-7} \times (T_e/300)^{-0.5}$
$H_2O+ + OH \rightarrow O + H_3O^+$	$8.21 \times 10^{-10} \times (0.62 + 0.4767 \times 5.5 \times (300/T_e)^{0.5})$
$H_2O + H_2O^+ \rightarrow OH + H_3O^+$	$9.26 \times 10^{-10} \times (0.62 + 0.4767 \times 5.41 \times (300/T_e)^{0.5})$
$H_2O^+ + HCO \rightarrow CO + H_3O^+$	$3.33 \times 10^{-1} \times 1.12 \times 10^{-9} \times (0.62 + 0.4767 \times 3.58 \times (300/T_e)^{0.5})$
$H_2O + OH^+ \rightarrow O + H_3O^+$	$4.64 \times 10^{-1} \times 9.39 \times 10^{-10} \times (0.62 + 0.4767 \times 5.41 \times (300/T_e)^{0.5})$
$H_3O^+ + O^- \rightarrow H + O + H_2O$	$3.76 \times 10^{-8} \times (T_e/300)^{-0.5}$
$H_3O^+ + OH^- \rightarrow H + OH + H_2O$	$3.76 \times 10^{-8} \times (T_e/300)^{-0.5}$

A4. Additional information obtained from the model

A4.1. Vibrational distribution functions for 20% H_2O

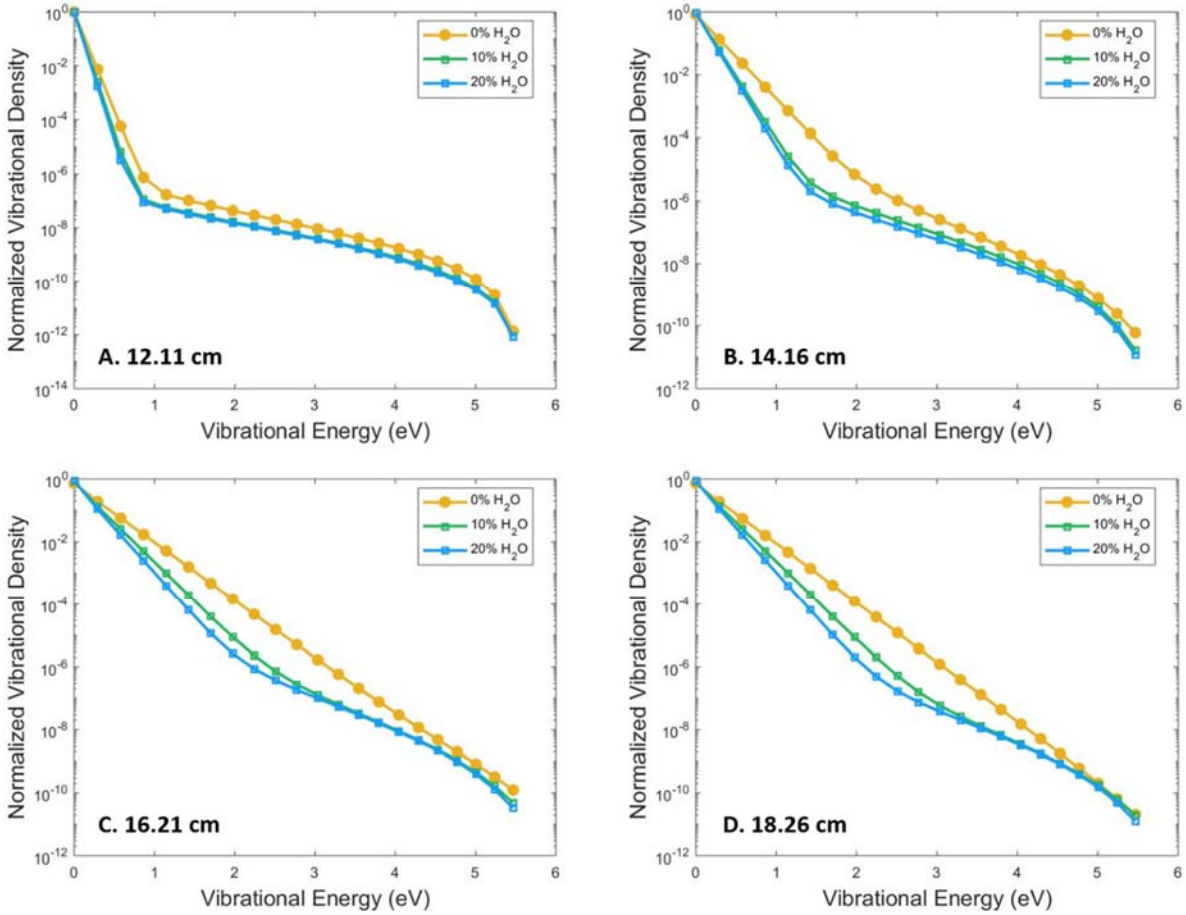

Figure A4.1 Calculated VDFs in pure CO_2, and upon 10% and 20% H_2O addition, at four different positions in the plasma tube (see figure 3 in the paper); it can be noted that the addition of more water leads to lower densities of CO_2 vibrational levels. However, for the higher levels, this effect is minimal.

A4.2. Influence of the Ion-Ion and Ion-neutral reactions

Interesting to mention is that the ion-ion and ion-neutral reactions added due to the water content change the densities of the secondary and tertiary species only by around 0.01% and have virtually no influence on the VDF. This is illustrated in figure A4.2 for the VDFs, which are plotted with and without ion-ion and ion-neutral reactions, showing that the VDFs virtually overlap.

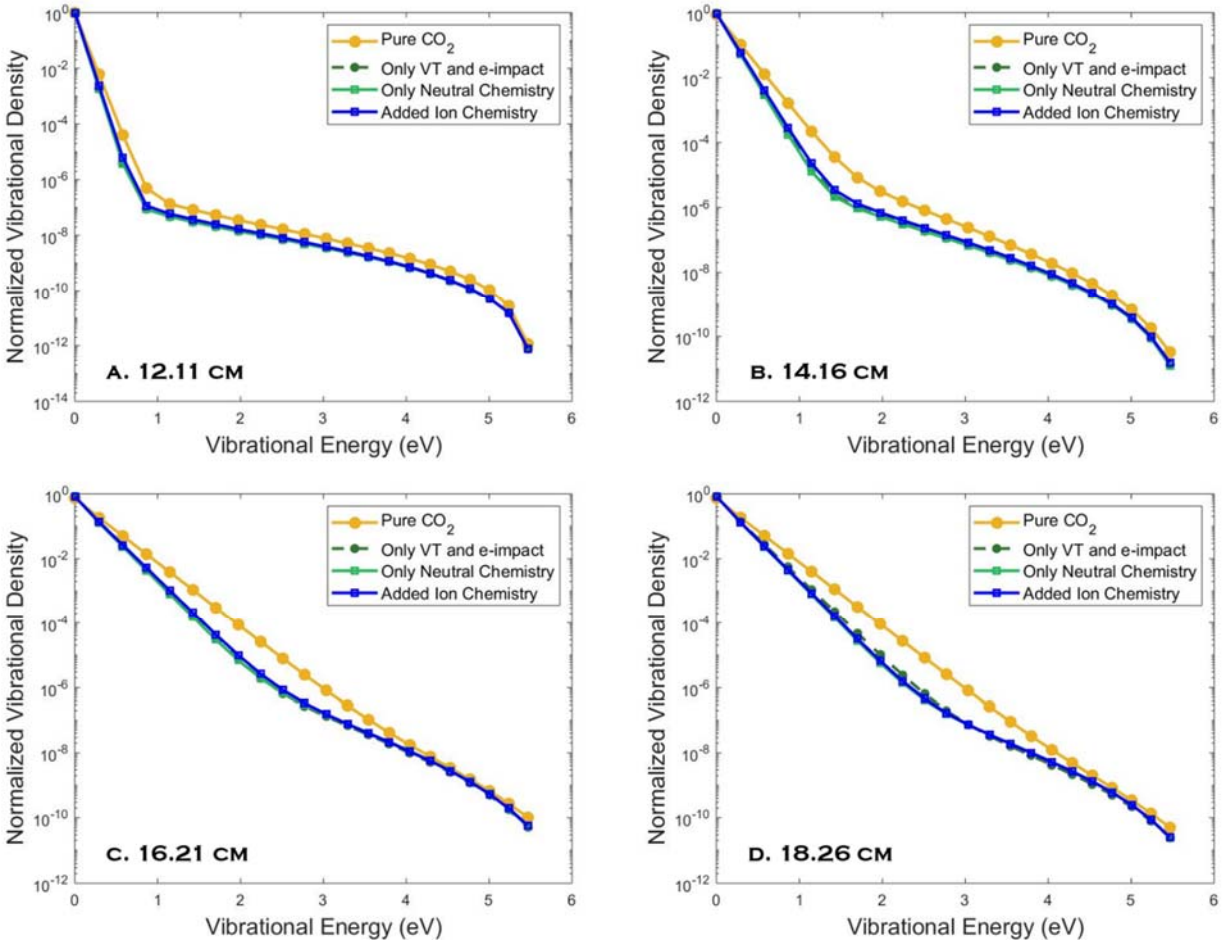

Figure A4.2 Calculated VDFs at different positions in the plasma, in pure CO_2, and upon addition of 10% H_2O, for different H_2O reactions added, i.e., only VT and electron impact reactions, and also adding the neutral and ion chemistry. It can be noted that the addition of more neutral, ion-neutral and ion-ion chemistry has no significant influence on the VDF.

A4.3. Influence of attachment – Electron density graph

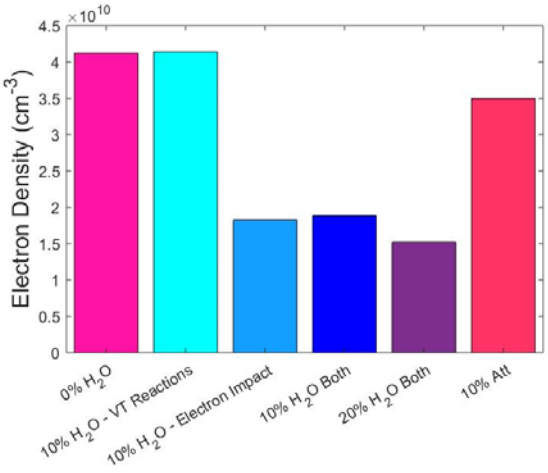

Figure A4.3 Influence of the reduction of the electron attachment rate to H_2O on the electron density; see last bar: By reducing the attachment rate to 10% of its default value, we observe a doubling of the electron density compared to the original case (CO_2 with 10% H_2O addition: dark blue bar). The other colour bars are the same as in Figure 6(B) in the main paper.

A4.4. Vibrational distribution functions for gas temperature influence

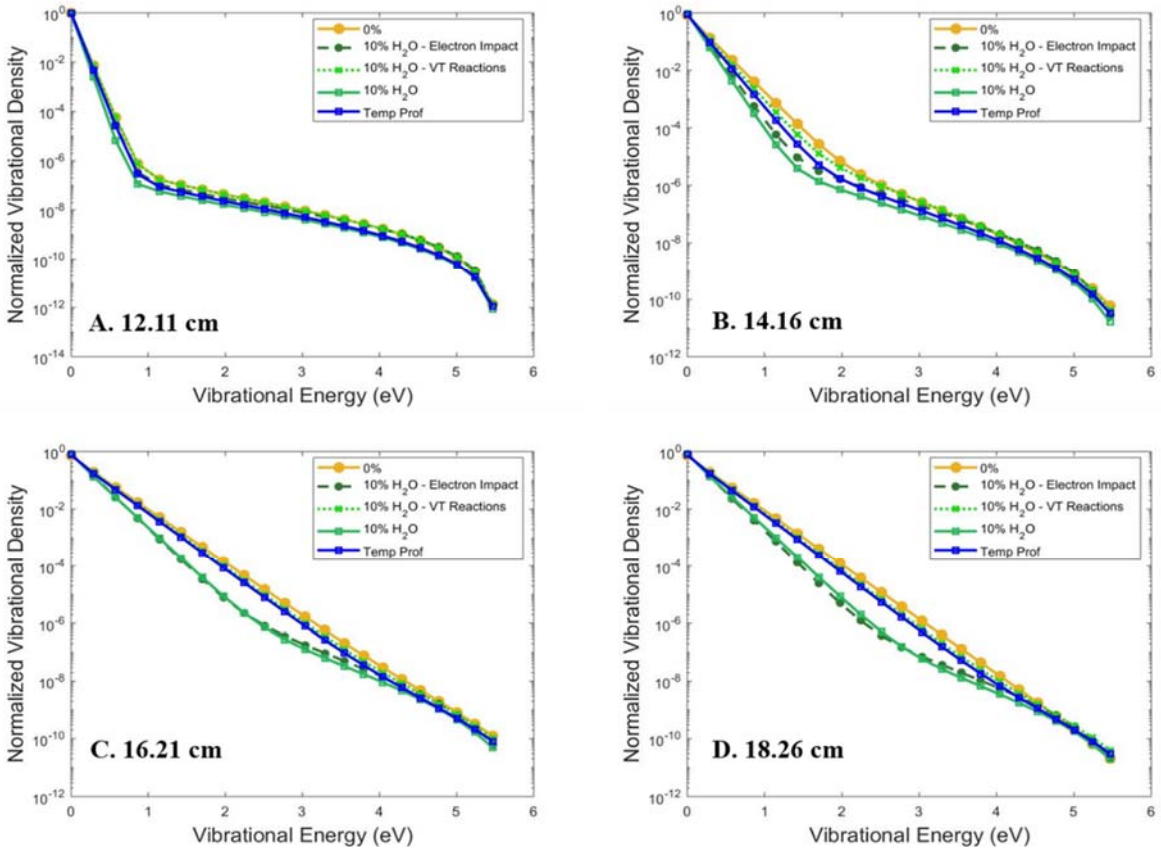

Figure A4.4 Influence of gas temperature on the calculated VDFs – If the temperature profile calculated in pure CO_2 is used in the CO_2/H_2O system, we can observe that the gas temperature only influences the VDF in the region before thermalisation, indicating that the gas temperature has no large effect on the VDF at the conditions under this study.

A4.5. Reaction rates for electron impact excitation

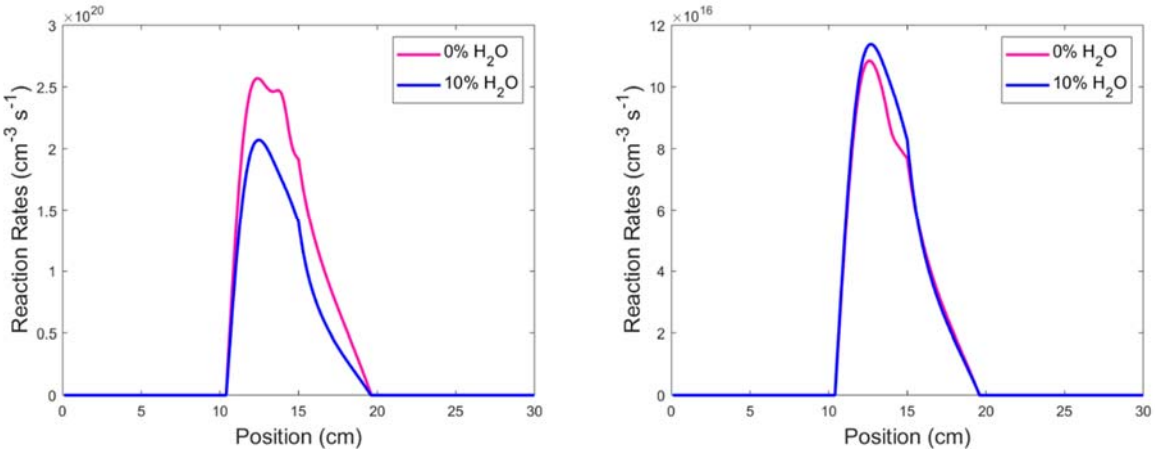

Figure A4.5. Calculated electron-impact vibrational excitation rates, for the sum of the lower levels (up to v = 16; left) and the sum of the higher levels (v ≥17; right), in pure CO_2 and for 10% H_2O addition.

A4.6. Influence of the parameters on the VDF

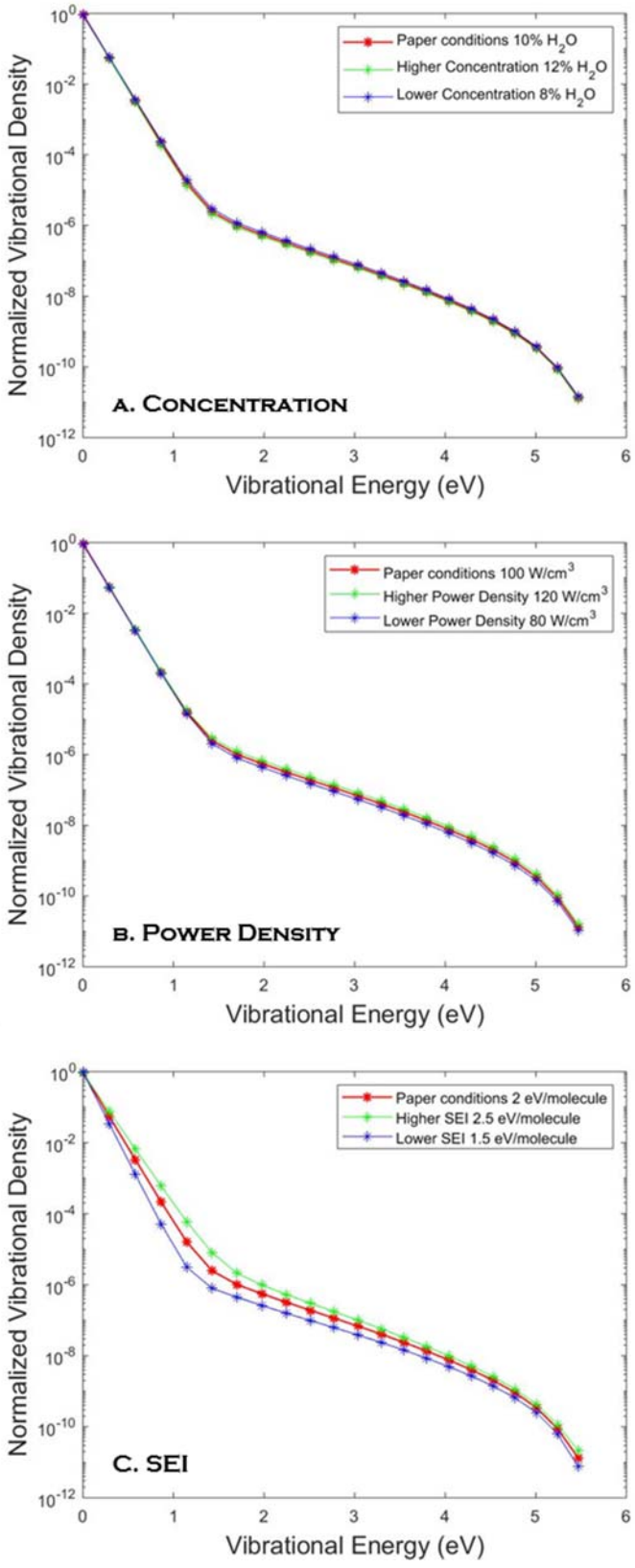

Figure A4.6. Influence of different parameters on the VDF: H_2O concentration (A), power density (B) , and SEI (C). Varying these parameters within the indicated range results in minor changes to the VDF.